Alma Mater Studiorum – Università di Bologna

DOTTORATO DI RICERCA IN
Meccanica e Scienze Avanzate dell'Ingegneria
Prog.3 Meccanica Applicata
Ciclo XXIV

**Settore Concorsuale di afferenza: 09/A2**

**Settore Scientifico disciplinare: ING-IND/13**

# New mechanisms for modelling the motion of the human ankle complex

**Presentata da:**
Ing. Benedetta Baldisserri

**Coordinatore Dottorato:**
Prof. Vincenzo Parenti Castelli

**Relatore:**
Prof. Vincenzo Parenti Castelli

**Esame finale anno 2012**

# Contents

CONTENTS

# Chapter 1

# Introduction

The *ankle complex* (for the definition see chapter 2) plays a fundamental role in human locomotion, being the junction between the shank and the foot. Thus, it is not surprising that ankle complex injuries are among the most common, particularly in sports. Because of its great importance for mobility and stability of human body during locomotor activity, the ankle complex has already been extensively investigated from anatomical, clinical and biomechanical points of view.

The understanding of human joint functions is provided mostly by *in vivo* and *in vitro* experiments. Nevertheless, ethical and technical reasons prevent adequately detailed measurement. Whereas *in vivo* studies should be limited, even in *in vitro* tests it is yet difficult to simulate and compare multiple conditions resulting from injury and surgical interventions. For these reasons, great attention has been devoted to modelling of human joints. Actually, models accurately reproducing certain characteristics of these joints are paramount. They help to understand or to discern many functional aspects that could be difficult to observe by means of standard experimental analyses. The forces exerted by the muscles and by the other articular components of the joint are a clear example of the difficulties which can be found within the practice. The experimental procedures and tools which are now available to measure these forces are highly invasive and do not make possible to obtain the required information. Nevertheless, the knowledge of the articular forces could be a support for clinical diagnoses and analyses; furthermore it could provide significant insights on the field of prostheses and orthoses [1].

According to this point, human joint models resulted also an effective aid in the design of innovative prostheses and orthoses. Joint models usefulness is not only the result of the amount of information given easily and quickly by any model. As in other applications, human joint models make possible indeed to reduce the cost of the prototyping stage, since they allow designers to foresee the behaviour of a prosthesis or an orthosis once it has been implanted on a patient. Moreover, the use of models during the design stage would reduce the number of *in vivo* or *in vitro* experimental tests needed to optimize a particular design or to fit the patient characteristics.

# CHAPTER 1. INTRODUCTION

Human joint models are either fundamental instruments in the surgical planning of an operation or during the operation itself. Some models are used together with with medical devices to customize or to modify prostheses and orthoses on an individual patient. Furthermore, human joint models allow surgeons to foresee the behaviour of a prosthetic joint, in particular when the original articular components are modified or removed at all. Finally, the use of efficient models could reduce the experimental tests on the patient and the post-operation interventions.

The attention on the ankle complex models has recently increased because of the poor results of total ankle replacement arthroplasty. These results caused the abandon of arthoplasty in the surgical practice and the subsequent return to arthrodesis (i.e. fusion of the joint). Several models of the ankle complex have been proposed but few studies have developed a kinematic, static or dynamic model of the ankle joint involving all the main anatomical structures (such as bones, ligaments, tendons, cartilage,...) playing an important role in the ankle's mechanical behaviour. Actually, the ankle joint static and dynamic behaviour has been investigated by several researchers using 2D models in which a hinge joint, representing the ankle complex, links together two rigid segments, one modelling the foot and the other one the lower leg. The low complexity of these models was consistent with the aim of the studies, for instance: studying the ankle strategy employed in balance control in [2,3], examining the correlation between ankle torque and ankle angle during walking to evaluate the implications for design of ankle prostheses in [4], testing the validity of a new ambulatory system for the measurement of the ground reaction force and the centre of pressure in [5,6]. However, recent accurate techniques have allowed the collection of experimental data showing instantaneous changing positions for the ankle joint axis of rotation, thus proving the unsuitability of such simple ankle complex models.

In the last few years, a new approach has been proposed for the modelling of human joints, which models the joint as *a linkage or an equivalent mechanism* whose geometry is based, as much as possible, on the joint's anatomical structures. The motion of the mechanism predicts the relative motion of the joint's main anatomical structures. These mechanisms are suitable to analyze the *passive motion* of the joint, that is the motion of the joint under virtually unloaded conditions (no external loads). This particular motion is believed to have a great relevance for a deeper understanding of the joint kinematics (see section 3.1).

In particular, planar [7,8] and spatial [9-13] mechanisms have been proposed for the simulation of the ankle passive motion. The comparison between experimental data and simulation results showed the efficiency of these models for the fitting both of the kinematic behaviuor and of the anatomy of the joint. Moreover, information obtained by these studies have been the rationale for the design of innovative ankle prostheses. However,

these mechanisms have several limitations: they rely upon some strong assumptions and take into account only a few anatomical structures of the ankle complex. In particular, the relative motion between tibia and fibula and between talus and calcaneus is not considered; furthermore, among all the ligaments of the ankle complex only the calcaneofibular and the tibiocalcaneal ligaments are modeled.

The aim of this thesis is to propose new equivalent mechanisms for the modelling of the ankle complex passive motion. The proposed models are directed to overcome the limitations of the previous ones. First of all the role of all the main ligaments of the ankle complex is investigated under virtually unloaded conditions by means of nine *5-5 fully parallel mechanisms*. In each mechanism, two of the five rigid links model two of the joint ligaments, while the remaining three links model the articular contact between talus and tibia and fibula. Moreover, based on the results obtained by this investigation, a new spatial equivalent mechanism of the lower leg is developed taking into account the fibula bone (here modeled as a rigid body with a relative motion with respect to the tibia bone), all the main ligaments of the ankle complex and the articulation between the fibula and the tibia at the proximal extremity. The goal of this mechanism is the replication of the passive motion of ankle complex by involving the main anatomical elements of the lower leg. In both the two investigations, simulation results are compared with experimental data, in order to show the efficiency of the approach and thus to deduce the role of each anatomical structure in the kinematic behavior of the ankle complex.

A brief anatomical description of the ankle complex is presented in chapter 2. The nine 5-5 fully parallel mechanisms and the new spatial equivalent mechanism for the simulation of the passive motion of the ankle complex are described in chapter 3 and 4 respectively.

# CHAPTER 1. INTRODUCTION

# Chapter 2

# Anatomy of the human ankle complex

This chapter gives some basic information about the ankle. Its scope is to describe the anatomical structures that are considered in the following. Furthermore, the nomenclature and the conventions adopted in this dissertation are presented. This paragraph is not meant to be a complete treatise about the human ankle, but a short and simple reference to clarify those points which are used in this dissertation.

## 2.1 The ankle components

The term *ankle* has been used with different meanings. In this thesis, the ankle joint refers to the *tibiotalar* (also referred to as *taloctural*) joint that is the multiple articulation between *tibia*, *fibula* and *talus* bones (Figure 2.1). As regards the articulation between tibia and talus, the internal region of the tibia distal surface (*mortise*) moves on the superior surface of the talus (*trochlea tali*) while the inner aspect of the lower extremity tibia (*medial malleolus*) moves on the medial surface of the talus. As regards the articulation between fibula and talus, the inner aspect of the lower extremity

**Figure 2.1:** The main structures which constitute the ankle complex [14].

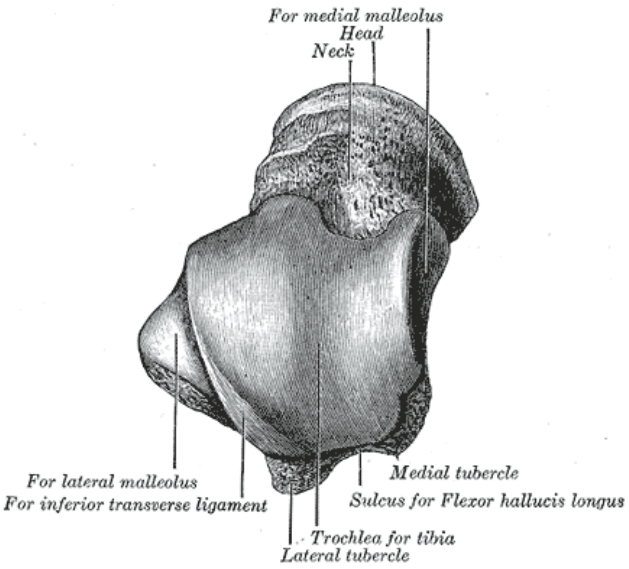


**Figure 2.2:** Left talus from above [15].

fibula (*lateral malleolus*) slides on the lateral surface of the talus.

The *subtalar* joint is the term used to refer to the connection between the inferior surface of the talus and the superior surface of the calcaneus. The *ankle complex* term is here used to mean the anatomical complex composed of the ankle and the subtalar joints, as defined above.

The ankle complex joint is formed by several anatomical parts which will be called *structures*, *elements* or *components* in the following, without distinction. They can be divided into passive and active structures. *Passive structures* are those elements which can exert forces only if externally stressed: articular surfaces, ligaments and other ligamentous structures belong to this category. On the contrary, *active structures* — such as the muscles — can intrinsically exert forces but, in general, they almost do not oppose external forces when inactive.

*Articular surfaces* are those parts of the bones which enter into mutual contact during ankle motion. In this case, they are the tibia mortise and the troclea tali, the medial malleolus and the talus medial surface, the lateral malleolus and the talus lateral surface, the inferior and the superior surfaces of talus and calcaneus respectively. For instance, the articular surfaces of the talus which compose the ankle joint are reported in Figure 2.2.

*Ligaments* are very important ankle elements which have a strong influence on the stability of the joint. They are composed by a fibrous connective tissue; that is why when only a part of the ligament is considered, it is referred to as a fibre or a bundle of fibres. The most important ligaments of the ankle complex provide a bone-to-bone

interconnection between the tibia, fibula, talus and calcaneus. The connective area between a ligament and a bone will be called *attachment* or *origin* and *insertion* in the following, without distinction.

The lateral aspect of the ankle is augmented by the *anterior (ant-TaFiL)* and *posterior (post-TaFiL) talofibular ligaments* and by the *calcaneofibular ligament (CaFiL)*. The medial side of the ankle complex joint is covered by the *deltoid ligament*, which originates on the medial part of the lateral malleouls and inserts on the navicular, talus and calcaneus. Because the origins and insertions of its different parts are contiguous and not sharply demarcated from each other, wide variations in its anatomical descriptions have been noted in the literature. In this thesis the deltoid ligament is divided into four bundles of fibres: the *tibionavicular ligament* (not considered in the models described in this dissertation), the *anterior (ant-TaTiL)* and *posterior (post-TaTiL) tibiotalar ligaments* and the *tibiocalcaneal ligament (TiCaL)*. Photographic images of these ligaments are presented in Figure 2.3: they were taken from a specimen, during an experimental section carried out at the Movement Analysis Laboratory of the Istituto Ortopedico Rizzoli (IOR).

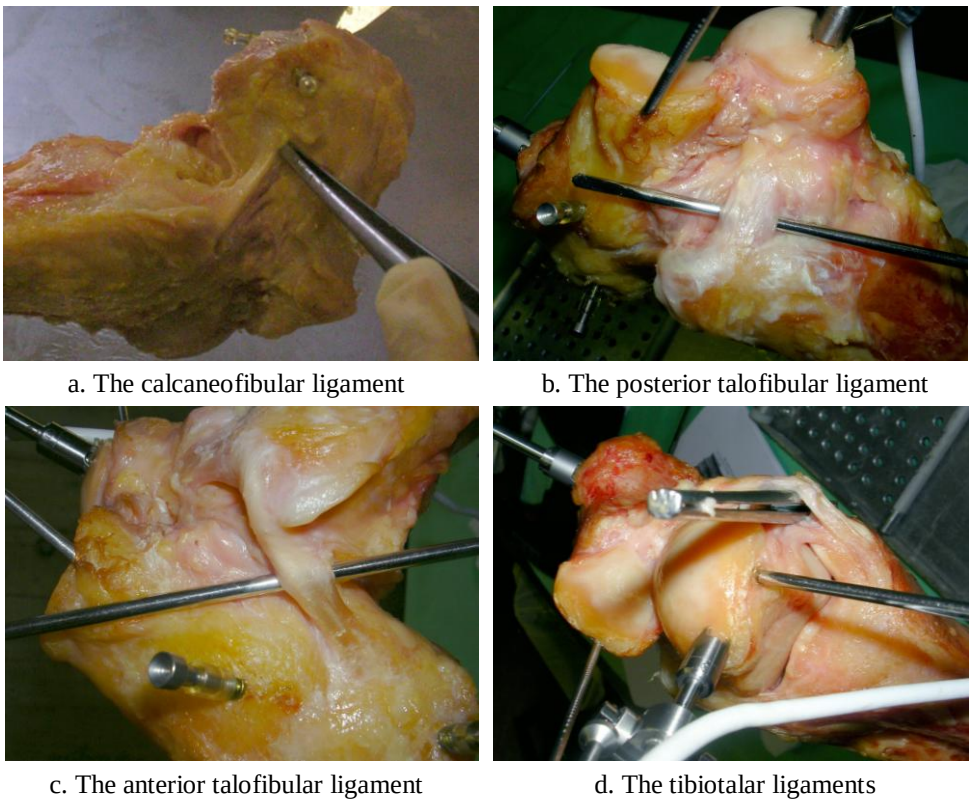

a. The calcaneofibular ligament

b. The posterior talofibular ligament

c. The anterior talofibular ligament

d. The tibiotalar ligaments

**Figure 2.3:** The principal ligaments of the ankle complex joint.

The set of ligaments and membranes that keep the tibia and the fibula together is also called *Syndesmosis*. In particular, the *interosseus membrane* is composed by fibres which originate in the indentation of the lateral end of the tibia and insert at the same level on the anterior two-thirds of the medial fibular surface (Figure 2.4).

Ankle muscles are not modelled in this dissertation, but a brief description is presented here. They are depicted in Figure 2. and Figure 2. . The anterior compartment of the tibia contains the dorsiflexors, or extensor, of the foot and ankle. The most important of these muscles is the *tibialis anterior*. The lateral compartment, surrounding the fibula, contains the *peroneal muscles*, which act as foot evertors and assist ankle plantarflexion. The posterior compartment contains the plantarflexors. The largest plantarflexors are the triceps surae which end in the calcaneal (Achilles) tendon, the largest and strongest tendon in the body. The *deep* muscles layer in the calf is composed of the flexor digitorum longus, the tibialis posterior and the flexor hallucis lungus.

**Figure 2.4:** The main passive structures which constitute the lower leg [14].

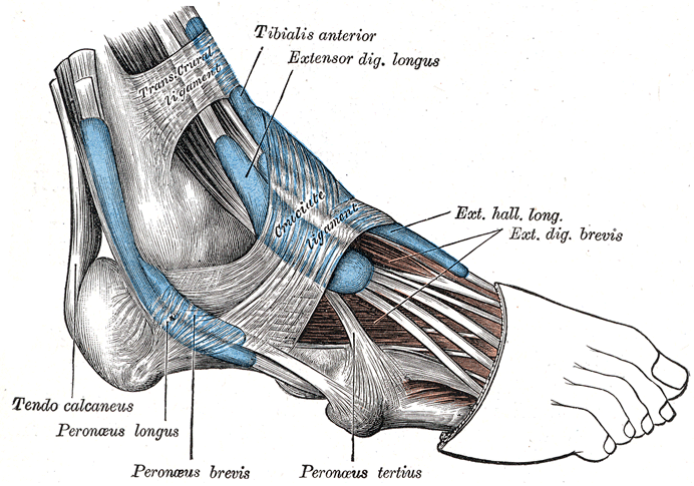


**Figure 2.5:** Lateral aspect of the ankle complex [15].

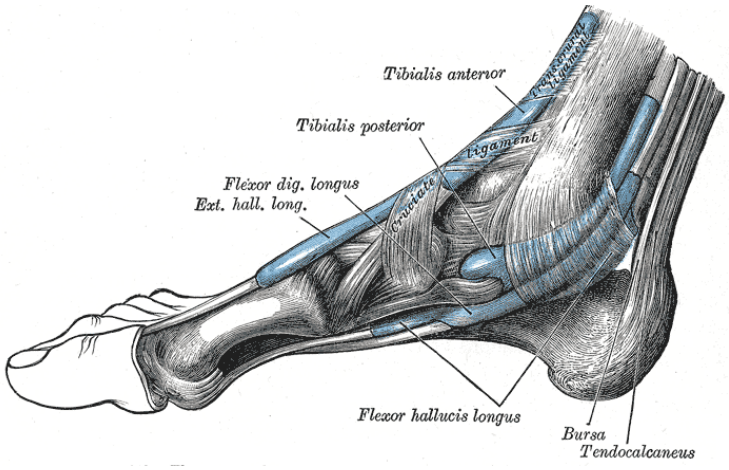


**Figure 2. 6:** Medial aspect of the ankle complex [15].

# CHAPTER 2. ANATOMY OF THE HUMAN ANKLE COMPLEX

# Chapter 3

# The modelling of the human ankle[1]

New models of the ankle complex joint are presented in this chapter. The approach based on equivalent mechanisms for passive motion modelling is introduced in section 3.1; the initial equivalent mechanism and the new ones representing the progress made by this work, are described in sections 3.2 and 3.3; finally, section 3.4 presents how the ankle motion is described is this dissertation.

## 3.1 Equivalent mechanisms for modelling the passive motion of human joints

The passive motion of the ankle complex joint is the relative motion of the tibia, fibula, talus and calcaneus bones when no loads (external or muscolar) are applied to the joint. It involves only some anatomical structures, i.e. the main passive structures of the joint.

The passive motion is believed to have a great relevance for a deeper understanding of the joint kinematics [17]. Indeed, for instance, with regard to the knee joint "the actual motion patterns of the human knee joint depend on a combination of its passive motion characteristics and the external loads" [18]. Moreover, the passive motion is considered a useful tool for a closer investigation of the role of the main anatomical structures of the joint (ligaments, articular surfaces, etc.) [19,20], which allows a more reliable dynamic analysis of the joint itself.

Since the particular loading condition of the passive motion can be considered as the simplest one which can be exerted on articulations, models of the passive motion of human joints are relatively simply. Thus, they are not difficult to interpret and can provide useful information for surgical treatments (in particular the design of total ankle replacement [21,22] and ligament reconstruction [23,24]), for rehabilitation issues and for designing prosthesis devices.

Several works showed that the passive motion of human joints can be replicated with good accuracy by equivalent mechanisms whose

[1] Part of the material described in this chapter has been published in [16].

geometry is based, as much as possible, on the joint anatomy. In particular, the motion of the mechanism predicts the relative motion of the joint's main anatomical structures under virtually unloaded conditions. Moreover, each rigid link corresponds to a specific anatomical element in order to make the geometry of the mechanism fit the anatomical structures of the natural joint. Several examples of equivalent mechanisms with one or more DOFs (degree of freedom) have been proposed in the literature to account for the knee and ankle passive motion [19,20,25,26,9,10,27,11,12,13,28,29]. Most of them are planar mechanisms and only a few are spatial. For example, one of the first spatial equivalent mechanism (with one DOF) for the study of the knee passive motion was presented in [19]. Remarkable results were also obtained in recent models which showed the power of combining a relative simplicity with the ability both to take the spatial motion of the articulation into good account and to fit the anatomical geometry [12,13,28,29].

As regards the ankle joint, planar [7,20] and spatial [9,11,12,13] equivalent mechanisms for the simulation of the joint passive motion have been recently proposed in the literature. All these mechanisms rely upon experimental measurements and show to be a good compromise between the fitting of the articulation passive motion and of the main anatomical structures of the ankle joint. In particular, very good results were obtained by the spatial mechanism presented in [11,13], which thus has been used as the start point of this work . This model is described in the next section 3.2.

## 3.2 The 5-5 FPM for modelling the passive motion of the ankle complex

In this section the model presented in [11,13] for the passive motion simulation of the ankle complex joint is briefly described. It is a spatial equivalent mechanism based on a one-to-one correspondence between the main anatomical structures of the ankle and the mechanism elements.

### 3.2.1 The kinematic model

The talus/calcaneus, considered as a single bone, and the tibia/fibula, also considered as a single bone, are modeled as rigid bodies. The tibia/fibula and the talus interfaces are considered in mutual contact at three points during flexion: at the lateral malleolus, at the internal region of the inferior surface of the distal tibia articulate with talus surface, and at the medial malleolus. Each contact surface is modeled as a spherical surface.

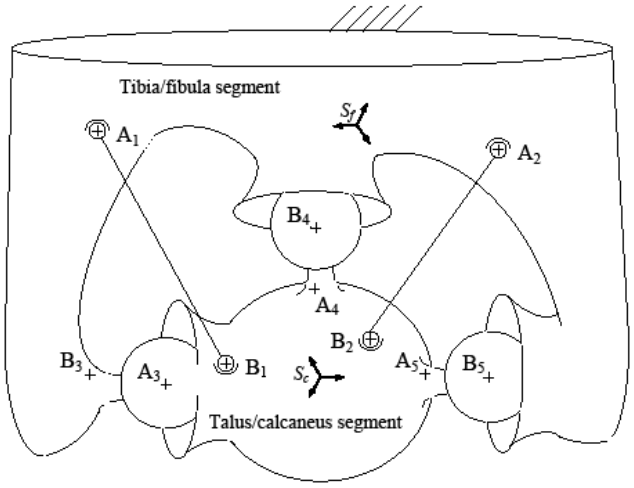


**Figure 3.1:** Schematic of the ankle complex joint.

Moreover, experimental data showed that some fibers of the CaFiL and the TiCaL ligaments are nearly isometric during the ankle passive motion [20]. According to this observation, the two ligaments are modeled by rigid binary links connected through spherical pairs to the bone segments.

The schematic of the ankle complex joint in Figure 3.1 relies upon these assumptions. Here points $A_i$ and $B_i$, $i$=1,2, represent the insertion on the two bone segments of two isometric fibres of the CaFiL and TiCaL ligaments respectively, while points $A_i$ and $B_i$, $i$=3,4,5, represent the centers of the mating spherical surfaces fixed to the talus/calcaneus and tibia/fibula respectively.

During the relative motion of the two ankle segments, each pair of mating spherical surfaces maintains the contact, therefore the distance $A_iB_i$, $i$ = 3,4,5, is constant. As a consequence, each pair of mating sphere can be modeled as a binary link connected to the bone segments through spherical pairs which are centered on the centers of the spheres.

Based on this consideration, a more synthetic equivalent mechanism for modelling the ankle complex is the one-DOF fully parallel mechanism of type 5-5 (*5-5 FPM*), i.e. a mechanism that features two rigid bodies interconnected by five bars of constant length via spherical joint (Figure 3.2). Here the meaning of the points $A_i$ and $B_i$, $i$ = 1,…, 5, is the same as in Figure 3.1.

The closure equations of the 5-5 FPM provide the relations between the dependent and independent variables of the motion. With reference to Figure 3.2, the closure equations can be easily found based on the consideration that each pair of points ($A_i$, $B_i$), $i$=1,…,5, are constrained to maintain a constant mutual distance $L_i$ during motion. This make it possible to write:

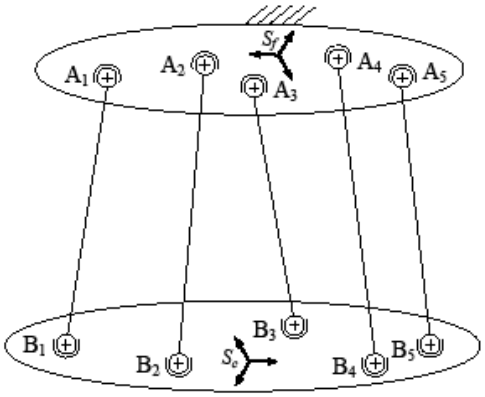


**Figure 3.2:** The 5-5 fully parallel mechanism.

$$\| \mathbf{A}_i - R \cdot \mathbf{B}_i - \mathbf{p} \|^2 = L_i^2 \quad (i=1,\ldots,5) \tag{3.1}$$

where $\mathbf{A}_i$ and $\mathbf{B}_i$ are the position vectors of the points $A_i$ and $B_i$, measured in the reference system $S_f$ and $S_c$ respectively. The Cartesian reference systems $S_f$ and $S_c$ are embedded in the based and in the platform respectively (see Figure 3.1 and Figure 3.2); they are defined as described in section 3.4. Vector **p** represents the position of the origin $O_c$ of the reference system $S_c$ with respect to the reference system $S_f$; matrix $R$ is the orthogonal rotation matrix 3x3 that transforms the components of a vector measured in $S_c$ into the components of the same vector measured in $S_f$. The matrix $R$ can be expressed as a function of three parameters α, β and γ that have been chosen for convenience to represent angles of rotations about three anatomical axes (the definition of the three angles is in section 3.4).
When considering the tibia/fibula as a fixed body, for a given geometry, system (3.1) can be regarded as a system of five nonlinear equations in six variables. These are the three components of vector **p** and the three orientation parameters which define the rotation matrix $R$. Given, for instance, the angle γ that measures the ankle flexion - i.e. the rotation between talus and tibia in the sagittal plane -, the remaining five variables can be found by solving the system (3.1).

### 3.2.2 The synthesis

The geometry of the equivalent 5-5 FPM is defined by 35 parameters: namely, 3·10 = 30 coordinates of the centres of the spherical pairs and 5 link lengths $L_i$, $i$=1,…,5. In order to find the optimal set of parameters and

the related mechanism, which allows the best simulation of the ankle experimental passive motion, a particular procedure was adopted [11,13].

This procedure starts from a first guess geometry of the mechanism that is defined using the measurement of the main anatomical structures of the ankle joint. The geometric parameters of the mechanism are then refined with an iterative process based on an error function *f* (objective function) that compares the poses of the movable bone segment obtained by the kinematic analysis of the mechanism, with the poses obtained by measurement data. This function is the sum of the weighted errors of the experimental values with respect to the calculated values, for the considered *n* values of the ankle flexion angle . In particular, the error function *f*, that is computed at each step of iteration, is defined as follows:

$$f = \sum_{j=1}^{5} \sum_{i=1}^{n} \frac{(x_{ji} - x^*_{ji})^2}{(x_{j\max} - x^*_{j\min})^2} \tag{3.2}$$

where, $x_{ji}$ is the actual value of the j-th dependent variable, $j$=1,…,5, at the i-th pose, $i$=1, …,$n$; $x^*_{ji}$ is the corresponding experimental value of the variable $xji$; $x_{jmax}$ and $x_{jmin}$ are the maximum and the minimum values of each of the dependent variables at the end of the process. Since the objective function is highly nonlinear and has discontinuities, the most traditional optimization methods, based on the gradient or on higher derivatives of the objective function and used to search for a relative minimum, do not provide good solutions to this problem. In the approach proposed in [11,13], the optimization problem is initially solved by means of a genetic algorithm; the obtained solution is then refined by means of a quasi-Newtonian algorithm.

Moreover, lower and upper bounds are introduced on the values of the 35 parameters, so that the points $A_i$ and $B_i$, $i$=1,…,5, that define the geometry of the equivalent mechanism, provide a final geometry of the optimized 5-5 FPM which retains the anatomical feature of the ankle complex (a more in-depth description of the optimization procedure is in Appendix).

## 3.3 The new 5-5 FPM models

Inspection of the ankle complex joint shows that the four bones (i.e. tibia, fibula, talus and calcaneus) are interconnected by a number of ligaments, which have not been considered in the 5-5 FPM modelling the joint passive motion (section 3.2). Namely, the four ligaments reported in Figure 3.3: the

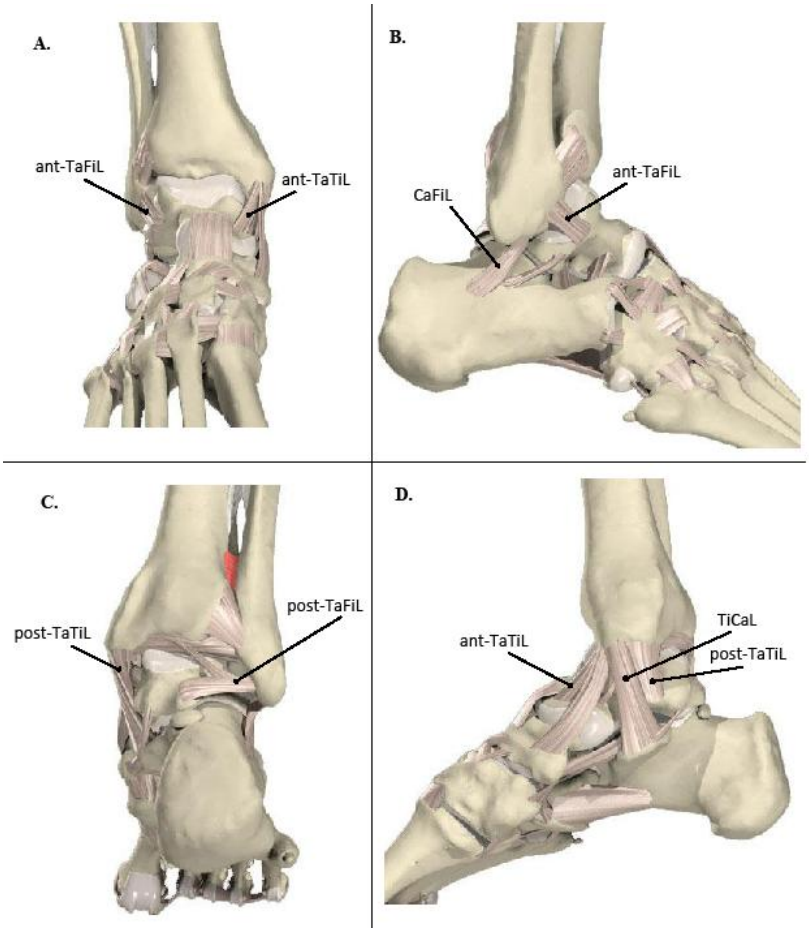


**Figure 3.3:** Schematic representation of the ankle complex joint: A. frontal view; B. lateral view; C. posterior view; D. medal view [14].

ant-TaTiL, post-TaTiL, ant-TaFiL and post-TaFiL ligaments. This observation gives rise the question on which role these ligaments are playing on the passive motion of the ankle joint. In fact, based on experimental evidence all these ligaments do not contrast the passive motion, i.e. they do not provide resultant forces to be balanced by external forces. On the other hand, it is quite improbable that all these ligaments are slack during the passive motion. In fact, this would be in contradiction with the ability (experimentally proved) of the joint to provide stiffness (which means that ligaments are recruited, i.e. deformed) in all directions as soon as the relative motion of the two main bones deviates from the passive one. These observations lead to formulate the hypothesis that these ligaments represent redundant constraints in the passive motion - that is they do not introduce forces -, which means that their length does not change during the motion. As a consequence they can be represented as isometric fibers during the passive motion. In other words, all ligaments when represented by the corresponding isometric fibers, allow the same passive motion. This makes

possible to consider any two of them to devise a 5-5 FPM of the ankle complex joint, still keeping the same three contact points of the two main bones.

In order to show the feasibility of the above mentioned hypothesis, in this work all combinations of the main ankle ligaments (including the TiCaL and CaFiL adopted in the 5-5 model presented in [11,13]) are selected to develop the corresponding synthesized 5-5 FPMs (sections 3.3.1 and 3.3.2). Moreover the results of the simulations obtained by each model are compared with the experimental data and the ability of the models to replicate the passive motion of the ankle joint is outlined (section 3.3.3).

### 3.3.1 Nine 5-5 FPMs for the ankle passive motion simulation

The new mechanisms developed to analyze the behavior of the main ankle ligaments are based on the same assumptions of the 5-5 FPM presented in [11,13]. As in [11,13] three points of contact are considered between the talus/calcaneus and the tibia/fibula segments, and the relative articular surfaces are approximated by spherical surfaces. Furthermore the isometric fibers of two ligaments out of six (i.e. the ant-TaTiL, post-TaTiL, ant-TaFiL and post-TaFiL ligaments) are also considered. Thus, by virtue of the considerations reported in the previous section, the equivalent mechanism can be represented by a 5-5 FPM as the one shown in Figure 3.2.

Therefore, by properly combining the six main ligaments, reported in the previous sections, different 5-5 FPMs can be devised. In particular, only the pairs comprising one lateral ligament and one medial ligament are taken into consideration in order to maintain a sort of symmetry in the position of the rigid rods of the mechanism; thus only nine 5-5 FPM models, **FPMi**, i=1,…,9, are analyzed. Namely:

- **FPM1**: ant-TaFiL and ant-TaTiL;
- **FPM2**: ant-TaFiL and TiCaL;
- **FPM3**: ant-TaFiL and post-TaTiL;
- **FPM4**: CaFiL and ant-TaTiL;
- **FPM5**: CaFiL and TiCaL (the same ligaments considered in [11,13]);
- **FPM6**: CaFiL and post-TaTiL;
- **FPM7**: post-TaFiL and ant-TaTiL;
- **FPM8**: post-TaFiL and TiCaL;
- **FPM9**: post-TaFiL and post-TaTiL.

### 3.3.2 Case study

The physical data necessary to synthesize the different equivalent mechanisms of the ankle complex joint, were taken from experimental

sessions. By the procedure shown in [11,13], the talocrural joint articular surfaces and the insertion areas of the CaFiL and TiCaL ligaments were obtained; the passive motion of the talus/calcaneus with respect to the tibia/fibula were also measured. In particular, the pose (position and orientation) of the trackers fixed to the tibia/fibula and the talus/calcaneus respectively were measured with respect to a Cartesian reference system fixed to the camera system used as acquisition system.

The anatomical data not provided by previous experiments - for instance, the insertion areas of ant-TaTiL, post-TaTiL, ant-TaFiL and post-TaFiL ligaments - were taken from the literature. In particular, the surfaces of tibia, fibula and talus bones taken from literature were scaled in a homogeneous way along the three Cartesian axes, in order to fit the talocrural joint articular surfaces previously measured (as an example, the result of this procedure is depicted in Figure 3.4 for tibia and fibula); the ligament insertions were then found on the obtained bone surfaces, using anatomical images and data.

For each mechanism, the same synthesis procedure described in the previous section 3.2.2 and presented extensively in [11,13] was adopted. That is, a guess geometry given, then an optimized geometry of the 5-5 FPM is obtained, which best fits the experimental and simulation relative tibia-talus passive motion. Inside the synthesis procedure, the insertion positions for each ligaments were bounded within a volume, the same for all ligaments, and chosen as to keep a closer anatomical relationship between the model parameters and the anatomical elements. Finally, the results of the ankle passive motion simulation (the relative passive motion between talus/calcaneus and tibia/fibula segments) obtained by the different mechanisms were compared with the same experimental data obtained by measurements (see the next section).

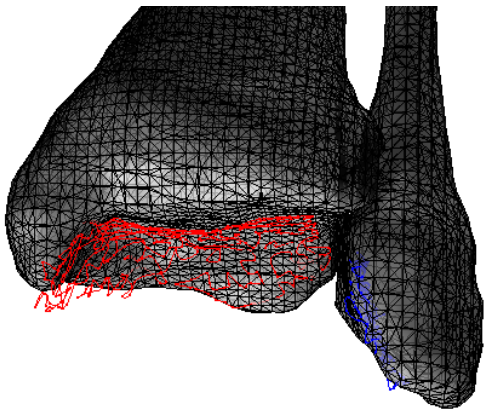

**Figure 3.4:** Tac of tibia and fibula fits the points of the articular surfaces of the two bones (red and blue respectively) which were digitalized during previous experimental sessions.

### 3.3.3 Comparison between simulations and experimental results

A synthetic representation of the comparison between model simulations and experimental results is reported in Figure 3.5 where, for the nine optimal models, the position error, the orientation error on angle α and the orientation error on angle β with respect to the experimental data, are reported versus the flexion angle γ.

The *position error* $E_{xyz,i}$ in the *i*-th configuration of the mechanism is defined as follow:

$$E_{xyz,i} = \sqrt{(x_i - x_i^*)^2 + (y_i - y_i^*)^2 + (z_i - z_i^*)^2} \tag{3.3}$$

where, $x_i$, $y_i$ and $z_i$ are the components of vector **p** (with reference to system (3.1)) calculated at the *i*-th mechanism pose, $i=1, \ldots, n$, and $x^*_i$, $y^*_i$ and $z^*_i$ are the corresponding experimental value of the variable $x_i$, $y_i$ and $z_i$.

The orientation error on angle α, *α error* $E_{\alpha,i}$, in the *i*-th configuration of the mechanism is defined as follow:

$$E_{\alpha,i} = \sqrt{(\alpha_i - \alpha_i^*)^2} \tag{3.4}$$

where the $\alpha_i$ angle is calculated at the mechanism *i*-th pose, $i=1,\ldots,n$, and $\alpha^*_i$ is the corresponding experimental value of the variable $\alpha_i$.

The orientation error on angle β, *β error* $E_{\beta,i}$, in the *i*-th configuration of the mechanism is defined as follow:

$$E_{\beta,i} = \sqrt{(\beta_i - \beta_i^*)^2} \tag{3.5}$$

where the $\beta_i$ angle is calculated at the mechanism *i*-th pose, $i=1,\ldots,n$, and $\beta^*_i$ is the corresponding experimental value of the variable $\beta_i$.

For a more synthetic representation of the results, in Table 3.1 the mean and the maximum value of the *position error*, $E_{xyz}$mean and $E_{xyz}$max, the mean and the maximum value of the *α error*, $E_{\alpha}$mean and $E_{\alpha}$max, the mean and maximum value of the *β error*, $E_{\beta}$mean and $E_{\beta}$max, for each of the nine models over the full range of the flexion angle, are reported.

A careful inspection of the results shows that all models replicate quite well the experimental passive motion. In particular, with reference to

Figure 3.5 and Table 3.1 the discrepancy on the rotation is lower than 1 degree for the prono/supination angle β, except for **FPM1** (black line) whose $E_{\beta}$max is 2.052 degrees - which is a low value as well -; for the intra/extra rotation α the discrepancy is lower than 1,5 degrees except for **FPM7** (yellow line) and **FPM8** (red line) whose $E_{\alpha}$max is in maximum dorsiflexion (2.544 and 3.269 degrees respectively). The global position error $E_{xyz,i}$ is contained within about 4.5 mm, specifically within 4.5 mm for **FPM1** (black line), **FPM7** (yellow line) and **FPM8** (red line), and within 2 mm for all the other models.

In conclusion, all the nine models showed to simulate the same passive motion pretty well, confirming that the whole system of the ankle complex joint comprises a number of ligaments which provide redundant constraints (the joint is therefore, conceptually, an overconstrained mechanism). A further step could be to investigate:

1. if the insertion points of the isometric fibers belong to a special 3-dimensional curve;
2. the role each **FPMi**, i=1,…,9, model has with respect to the ankle stability.

| | $E_{xyz}$mean [mm] | $E_{xyz}$max [mm] | $E_{\beta}$mean [degrees] | $E_{\beta}$max [degrees] | $E_{\alpha}$mean [degrees] | $E_{\alpha}$max [degrees] |
|---|---|---|---|---|---|---|
| **FPM1** | 3.689 | 4.418 | 0.960 | 2.052 | 0.504 | 1.127 |
| **FPM2** | 0.679 | 1.305 | 0.147 | 0.774 | 0.275 | 0.712 |
| **FPM3** | 1.216 | 2.155 | 0.086 | 0.232 | 0.418 | 1.005 |
| **FPM4** | 0.899 | 1.531 | 0.210 | 0.939 | 0.489 | 1.212 |
| **FPM5** | 0.600 | 1.215 | 0.112 | 0.744 | 0.398 | 1.355 |
| **FPM6** | 0.636 | 1.258 | 0.093 | 0.417 | 0.599 | 1.337 |
| **FPM7** | 2.824 | 4.259 | 0.153 | 0.673 | 0.566 | 2.544 |
| **FPM8** | 1.843 | 3.709 | 0.295 | 1.090 | 0.737 | 3.269 |
| **FPM9** | 0.672 | 1.281 | 0.109 | 0.588 | 0.566 | 1.354 |

**Table 3.1:** Kinematic errors of the different 5-5 FPM: $E_{xyz}$mean and $E_{xyz}$max are the mean value and the maximum value of the position error respectively, $E_{\alpha}$mean and $E_{\alpha}$max are the mean value and the maximum value of the α error respectively, $E_{\beta}$mean and $E_{\beta}$max are the mean value and the maximum value of the β error respectively.

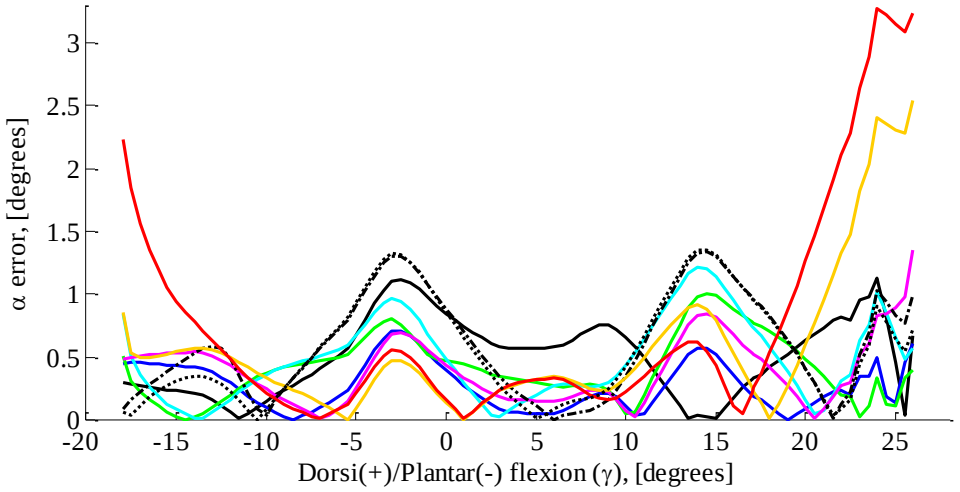


a.

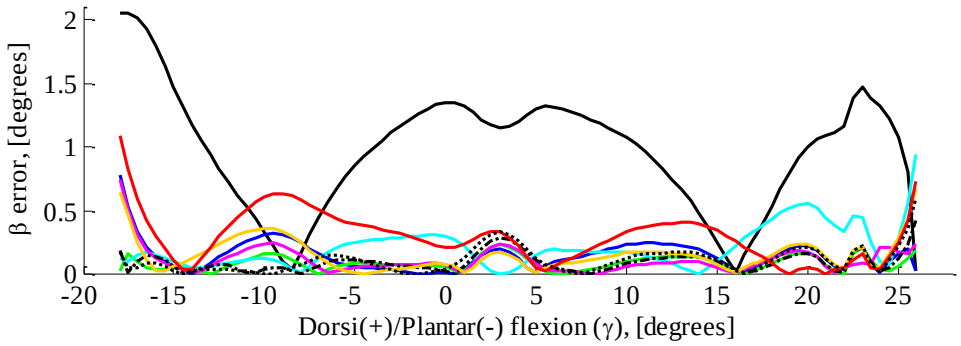


b.

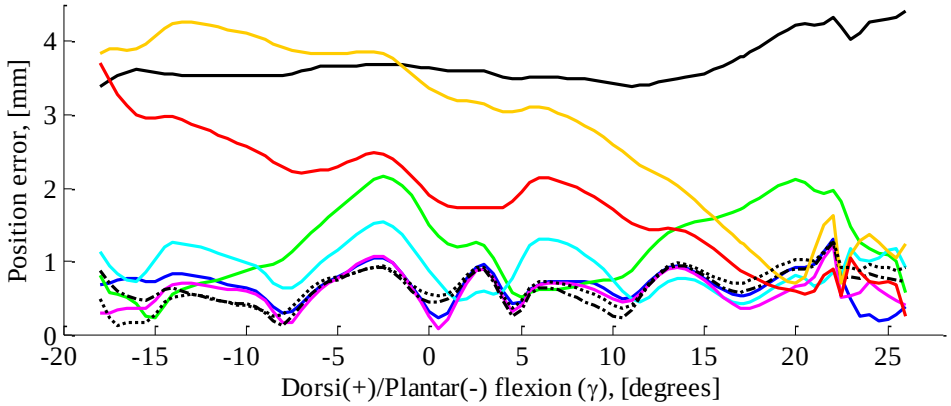


c.

**Figure 3.5:** Kinematic errors for the different equivalent mechanisms, versus ankle's flexion angle γ: black line is **FPM1**, blue line is **FPM2**, green line is **FPM3**, cyan line is **FPM4**, magenta line is **FPM5**, black dashdot line is **FPM6**, yellow line is **FPM7**, red line is **FPM8**, black dotted line is **FPM9**.

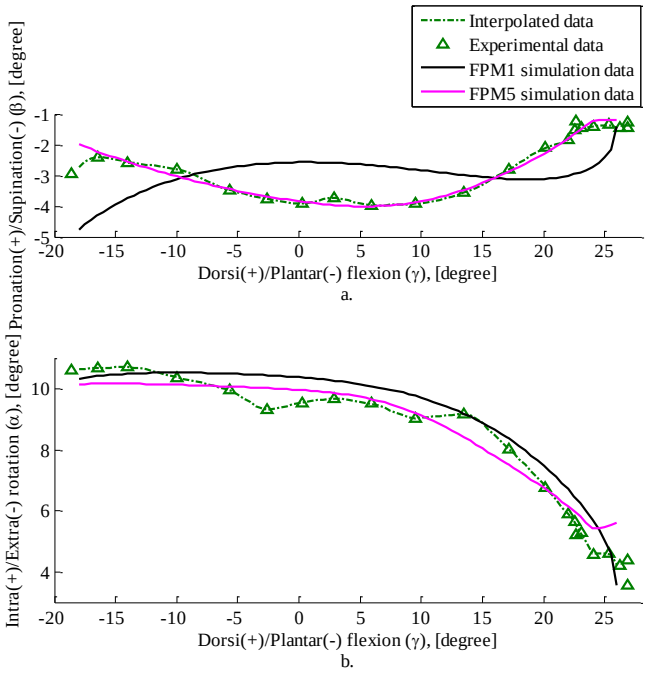


**Figure 3. 6:** Passive simulation of the talus/calcaneus respect to the tibia/fibula: angles β, (a.), and α, (b), versus ankle's flexion angle γ.

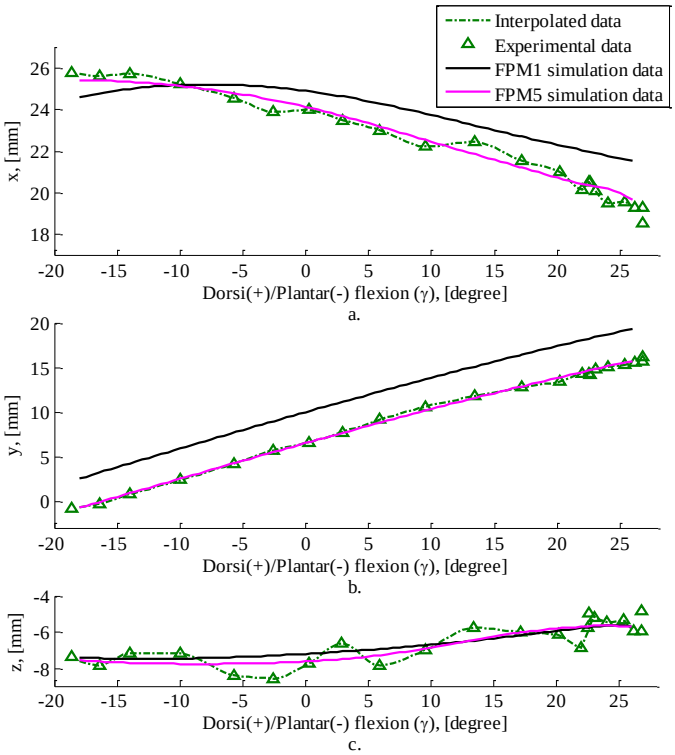


**Figure 3.7:** Passive simulation of the talus/calcaneus respect to the tibia/fibula: x, (a), y, (b), and z, (c) versus ankle's flexion angle γ.

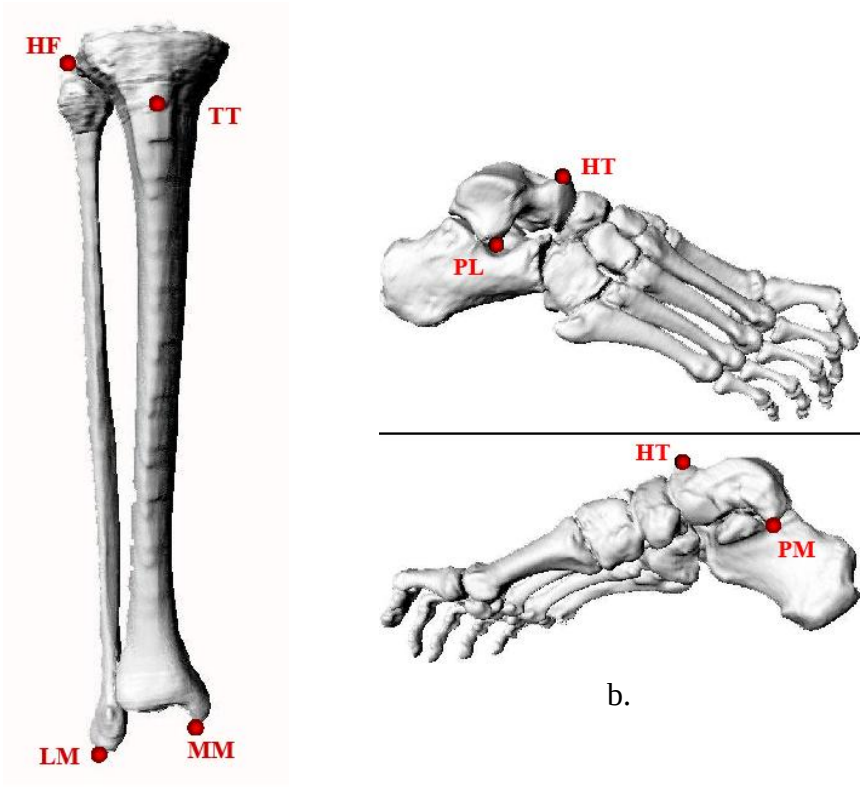


a. b.

**Figure 3.8:** The anatomical points for the definition of the tibia/fibula anatomical frame (a.) and the talus anatomical frame (b.).

## 3.4 The description of the ankle complex motion

In order to identify every point of the joint, it is necessary to define reference frames. In particular, it is convenient to define two anatomical frames attached to the tibia/fibula and talus respectively: the coordinates of a point of a bone segment expressed in the corresponding anatomical frame do not change with ankle configuration. Moreover, the relative pose (position and orientation) between tibia/fibula and talus can be described by means of the kinematic parameters which define the relative poses of the corresponding reference frames. Since the calcaneus is considered as rigidly attached to the talus, these two bones share the same anatomical frame.

The anatomical frames of tibia/fibula and talus were determinated starting from some anatomical points easily recognizable, which are depicted in Figure 3.8.

The tibia/fibula anatomical frame ($S_f$) was defined as follows (Figure 3.9):

- origin: located at the midpoint, IC, of the line joining the lower ends, LM and MM, of the tip of the lateral and medial malleolus respectively;
- y-axis: the line intersection between the quasi-frontal plane (defined by the tip of the malleoli and the head of the fibula HF) and the quasi-sagittal plane (orthogonal to the quasifrontal plane and passing through the point IC and the tibial tuberosity TT), and pointing proximally;
- x-axis: the line perpendicular to the quasi-frontal plane and pointing forward;
- z-axis: as a consequence, according to the right hand rule.

Likewise, the talus anatomical frame ($S_c$) was defined as follows (Figure 3.9):

- origin: coincident with the midpoint, IP, between the points PL and PM, respectively the tips of the lateral and medial posterior surface of the talus;
- y-axis: the line perpendicular to the quasi-transverse plane (defined by the the tips of the lateral and medial posterior surface of the talus, and the head of the talus HT), and pointing proximally;
- x-axis: the line connecting the head of the talus and the origin IP, and pointing forward;
- z-axis: as a consequence, according to the right hand rule.

The three rotation axes, that define the joint coordinate system necessary to describe the orientation of the talus with respect to the tibia/fibula, were chosen with the desirable characteristic that joint rotations are independent of the order in which the component rotations occur. For this reason a convention deduced by the Grood and Suntay joint coordinate system [30] was used: the $z_f$ axis of $S_f$ fixed to the tibia/fibula as the first one, the $y_c$ axis of $S_c$ fixed to the talus as the second one, finally an axis coincident with the shortest distance straight line of the other two axes as the third one. Three angles about these axes were defined as follows: the ankle dorsiflexion(+)/plantarflexion(-) angle $\gamma$ about the z-axis of $S_f$ , the ankle internal(+)/external(-) rotation angle $\alpha$ about the y-axis of $S_c$, and the ankle pronation(+)/supination(-) angle $\beta$ about a floating axis defined by the cross vector product of the unit vectors of the z-axis of $S_f$ and the unit vector of the y-axis of *Sc*.

According to this convention, the rotation matrix *R* was obtained:

$$R = \begin{bmatrix} c_\alpha c_\gamma - s_\alpha s_\beta s_\gamma & -c_\beta s_\gamma & s_\alpha c_\gamma + c_\alpha s_\beta s_\gamma \\ c_\alpha s_\gamma + s_\alpha s_\beta c_\gamma & c_\beta c_\gamma & s_\alpha s_\gamma - c_\alpha s_\beta c_\gamma \\ -s_\alpha c_\beta & s_\beta & c_\alpha c_\beta \end{bmatrix} \tag{3.6}$$

where *c* and *s* indicate the cosine and sine of the angle in subscript. In order to maintain the clinical meaning for the rotations (α, β, γ), if considering a right leg, the sign of the angle β should be inverted in (3.6), while, if considering a left leg, the sign of the angle α should be inverted in (3.6). It is worth noting that even though the Grood and Suntay convention was originally defined for the tibiofemoral joint, its application on different joints (the patello-femoral joint included) is becoming ordinary in the scientific literature.

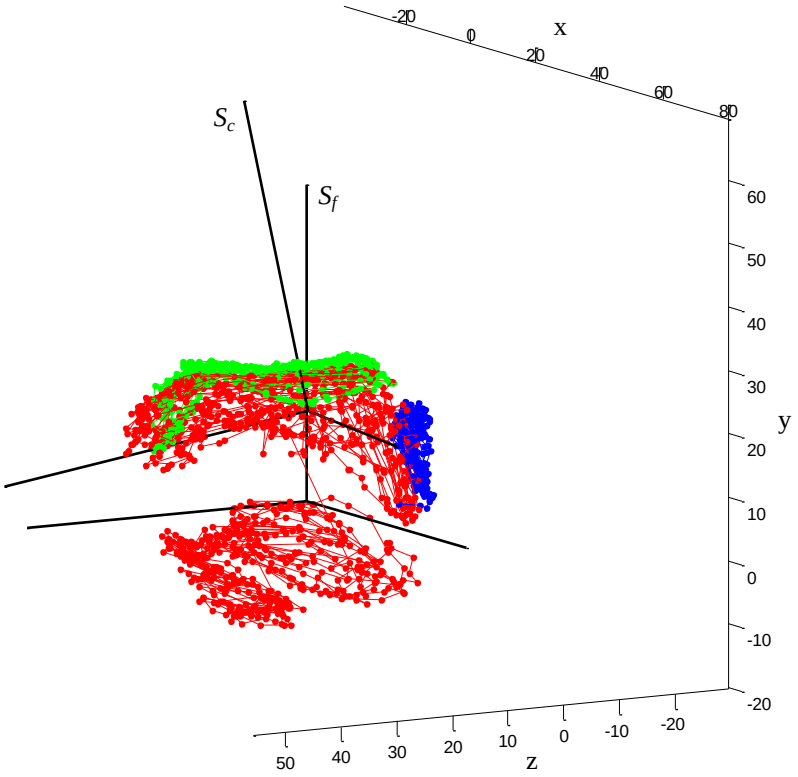


**Figure 3.9:** The two anatomical frames $S_f$ and $S_c$ (black) represented together with the tibial (green), fibular (blue) and talar (red) articular surfaces.

# CHAPTER 3. THE MODELLING OF THE HUMAN ANKLE

# Chapter 4

# The modelling of the human lower leg[1]

A deeper understanding of the ankle complex behavior and role in human locomotion needs the study on the interaction between the anatomical structures of the joint and the other ones that constitute the whole lower leg. For instance, since the fibula bone is directly involved in the ankle kinematic and dynamic behavior [35-41], the investigation of the fibula role during the ankle motion both in passive conditions and in response to external loads can provide useful information about the articulation. One example is the new computational model of the lower limb presented in [42] and developed to study the effects of a syndesmotic injury on the relative motion between tibia and fibula, and the ankle inversion stability. The modelled anatomical elements are several bones (the whole tibia and fibula, talus and calcaneus, navicular, cuneiform and metatarsal bones), several ligaments and the interosseus membrane. In particular, bones are represented with rigid bodies in mutual contact - ignoring articular cartilage deformation – and ligaments and the interosseus membrane by linear springs. This new computational model seems to be almost an exception, because the great majority of kinematic or dynamic models of the human lower limb that can be found in the literature represent the ankle joint as an ideal hinge joint or a spherical joint that links together two rigid segments corresponding to the foot and the lower limb [43-51].

This work focuses on the kinematic modelling of the ankle complex joint by means of spatial mechanisms that take into account several anatomical structures of the lower leg: namely, the main ligaments and the articular contacts. In particular, a spatial equivalent mechanism is sought for the simulation of the passive motion of an articulation that involves four bones: tibia, fibula, talus and calcaneus. In this anatomical complex, the ankle joint plays a fundamental role.

It needs to underline that the successful approach based on equivalent mechanisms for modelling the human joint passive motion (see section 3.1) allows the use of different valid solutions for the development of the sought-for equivalent mechanism. Actually, it involves two main choices: which anatomical structures of the articulation will be taken into account and how these structures will be modeled. The two choices have a

[1] Part of the material described in this chapter has been published in [31-34].

degree of arbitrariness, which means that different mechanisms can be devised in order to simulate the passive motion of an articulation. Each of these feasible models has an its own target that depends on the features of the mechanism as, for instance:

- giving information about the behavior of some particular ligaments during the joint motion;
- describing the articular contacts, that is a basic skill for the analysis of the articulation when external forces are applied;
- better replicating the relative motion of the joint bones.

Thus, in section 4.1 a preliminary study is presented in which some assumptions are defined, on which the devising of equivalent mechanisms for the simulation of the lower leg passive motion is based, and two preliminary one-DOF spatial mechanisms are presented. In section 4.2 the efficiency of the proposed equivalent mechanism is shown by the comparison between simulation results and experimental data.

## 4.1 Preliminary study

### 4.1.1 Modelling basic assumption

The efficiency of the approach based on equivalent mechanisms for modelling the passive motion shows that if a close correspondence between articulation anatomical structures and mechanism elements can be recognized, then a useful equivalent mechanism can be devised, which satisfactorily simulates the passive motion of the articulation.

In this work, the following correspondences are assumed in order to devise the equivalent mechanism for the lower leg passive motion simulation:

1. bones with rigid bodies. In particular, talus and calcaneus are considered as a single rigid body because the relative motion between the two bones is negligible with respect to the relative motion of the other bones [7,20];
2. ligament isometric fibres with rigid rods. Actually, till now only TiCaL and CaFiL ligaments showed an isometric behavior during passive flexion in experimental sessions [20]; for the other ligaments, the isometry of some fibres is taken as an assumption which is strongly justified by results shown in chapter 3;
3. ligament-to-bone insertions with spherical pairs (or universal joints for also considering the ligaments twisting around their own axes);
4. bone contact points with higher pairs which have 5-DoFs. For instance, sphere-on-sphere contact higher pairs are equivalent to two rigid bodies linked by a rigid rod connected to the two bodies by spherical pairs (this consideration is used for mechanisms described in chapter 3). Actually,

during the relative motion of two conjugated spherical surfaces, the two surfaces maintain the contact at a single point and the distance between the centres of the two spheres does not change.

Furthermore, experimental studies showed that during passive joint flexion, the ankle complex behaves as a one-DOF system [7,20,11,12,13]. Based on this observation, it is assumed that the lower leg can also be considered as a one-DOF system under virtually unloaded conditions.

### 4.1.2 Intermediate models

Several feasible one-DOF spatial equivalent mechanisms can be developed for the simulation of the lower leg passive motion which are based on the assumptions presented above. If, for instance, all contacts between the bones are modelled as sphere-on-sphere higher pairs, they can be represented with rigid rods linked to the bones by spherical pairs, the same as for the ligament isometric fibres. It can be easily shown by the Kutzbach formula [52] that a mechanism with three rigid bodies (tibia, fibula and talus/calcaneus segments) interconnected by binary links through spherical pairs requires 11 binary links connecting the three segments in order to have one-DOF.

The 11 rods and the three rigid bodies can be arranged to form different mechanisms according to how the bone contacts are modelled and consequently how many ligaments are considered. Indeed, the adopted model for the articular surfaces of the bones involved in the articulation determines how many binary links have to be used to represent bone contact points and consequently how many ligament isometric fibres should be used.

For instance, two possible one-DOF spatial mechanisms are shown in the schematics of the lower leg depicted in Figure 4.1 for the simulation of the passive motion: the three segments modelling the bones are interconnected to each other by black dots, representing bone contacts, and rigid rods ending with spherical pairs, representing ligament fibres.

In the first schematic of the lower leg modelled by **M1** equivalent mechanism (Figure 4.1a), at the ankle joint four higher pairs model the articulation of talus with fibula and tibia: one at the medial malleolus between talus and tibia, one at the internal region between talus and tibia and two at the lateral malleolus between talus and fibula; instead, one higher pair models the contact between tibia and fibula at their proximal end. Moreover, the band of ligament fibres which spread out on the medial malleolus from the apex of the tibia to the talus (*TaTiL ligament*) is modelled as a rigid rod, that is connected through spherical pairs to the bone segments. Thus, in the schematic of Figure 4.1a the three rods at the ankle joint represent TiCaL, TaTiL and CaFiL ligaments. Finally, the interosseus

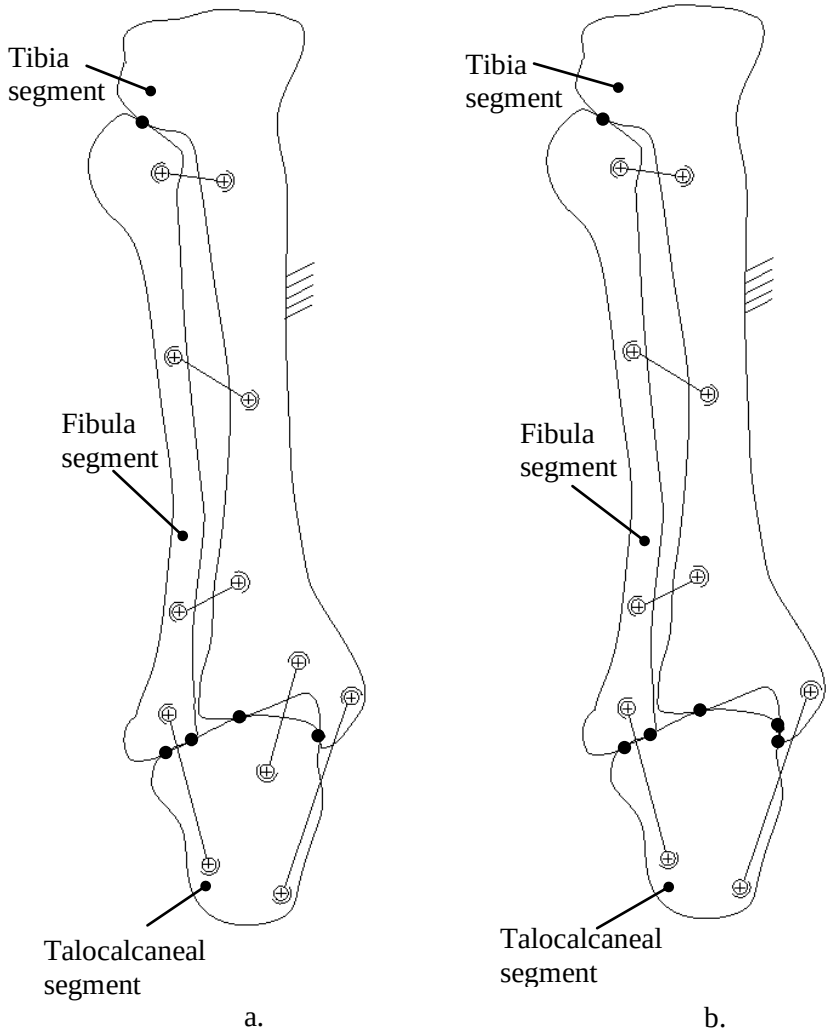


**Figure 4.1:** Schematics of the lower leg with **M1** (a.) and **M2** (b.).

membrane between tibia and fibula is modeled as three rigid binary links connected through spherical pairs to the bones.

In the second schematic of the lower leg modelled by **M2** equivalent mechanism (Figure 4.1b), at the ankle joint five higher pairs model the articulation of talus with fibula and tibia: two at the medial malleolus between talus and tibia, one at the internal region between talus and tibia and two at the lateral malleolus between talus and fibula; instead, one higher pair models the contact between tibia and fibula at their proximal end. Moreover, in the schematic of Figure 4.1b the two rods at the ankle joint represent TiCaL and CaFiL ligaments. Also here the interosseus membrane between tibia and fibula is modeled as three rigid binary links connected through spherical pairs to the bones.

## 4.2 The equivalent mechanism for modelling the lower leg passive motion

Both models shown in Figure 4.1a and Figure 4.1b could be adopted for the modelling of the lower leg passive motion thanks to the presented approach. However, in the previous work on the simulation of the ankle complex passive motion [11,13], the contacts of the talus with the tibia and fibula were successfully modelled as two sphere-on-sphere higher pairs and as one sphere-on-sphere higher pair respectively. Moreover, the study described in chapter 2 showed that the main ligaments of the ankle joint can be considered as redundant constrains when no external forces are applied, thus they can be modelled by rigid binary links for the ankle passive motion

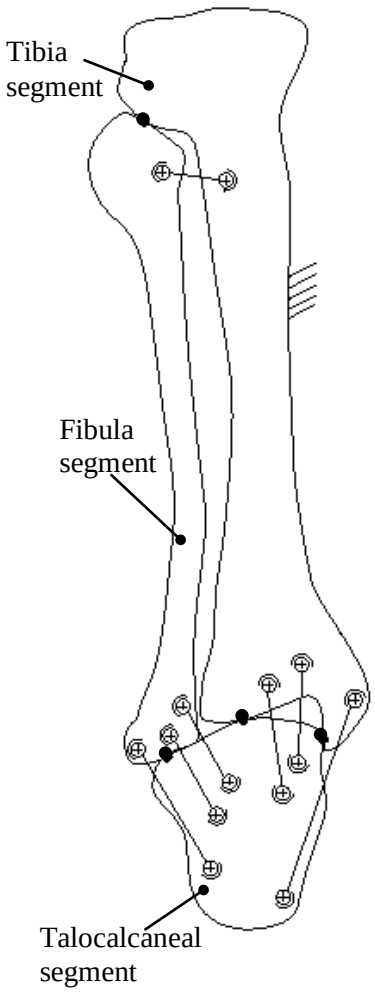


**Figure 4.2:** Schematic of the lower leg with **M3**.

simulation.

Therefore, by using these assumptions both for bone contacts and for the main ligaments at the ankle joint, a further new model of the lower leg can be devised, which is simpler than the two previous ones. The new spatial one-DOF mechanism **M3** proposed for modelling the lower leg passive motion is described in section 4.2.1; sections 4.2.2 and 4.2.3 report the kinematic analysis and the procedure for the synthesis of the mechanism respectively; comparison between simulations and experimental results are presented in section 4.2.4.

## 4.2.1 The equivalent mechanism

The schematic of the lower leg modelled by **M3** equivalent mechanism is depicted in Figure 4.2. As it is explained above, the talus and the tibia bones are considered in mutual contact at two points (at the medial malleolus and at the internal region of the inferior surface of the distal tibia articulated with the talus surface), while the talus and the fibula bones are considered in mutual contact at one point (at the lateral malleolus). The portion of each contact surface is approximated by a spherical surface. Moreover, based on a careful inspection of the proximal part of the tibia and the fibula, the connection between the two bones surfaces is modelled as a plane-to-sphere contact higher pair (see Figure 4.3).

The main ligaments of the ankle complex joint (see Figure 3.3) are represented as rigid rods connected to bone segments by spherical pairs, i.e:

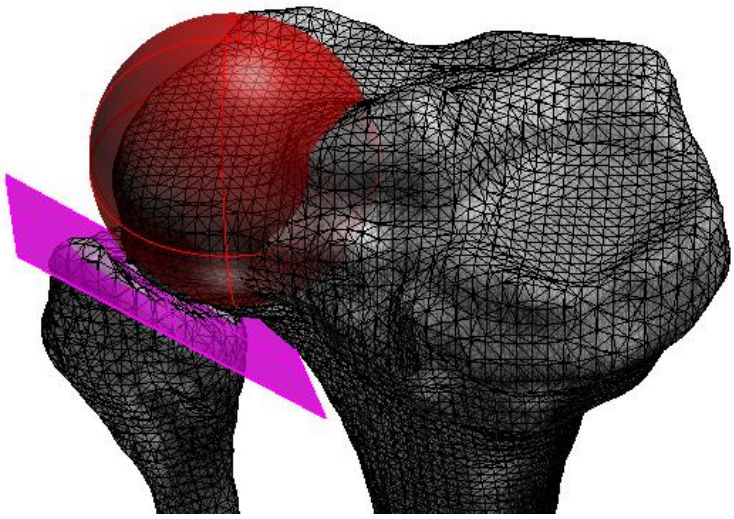

**Figure 4.3:** The articular contact between tibia and fibula at their proximal end. The approximation by spherical and planar surfaces respectively is also presented.

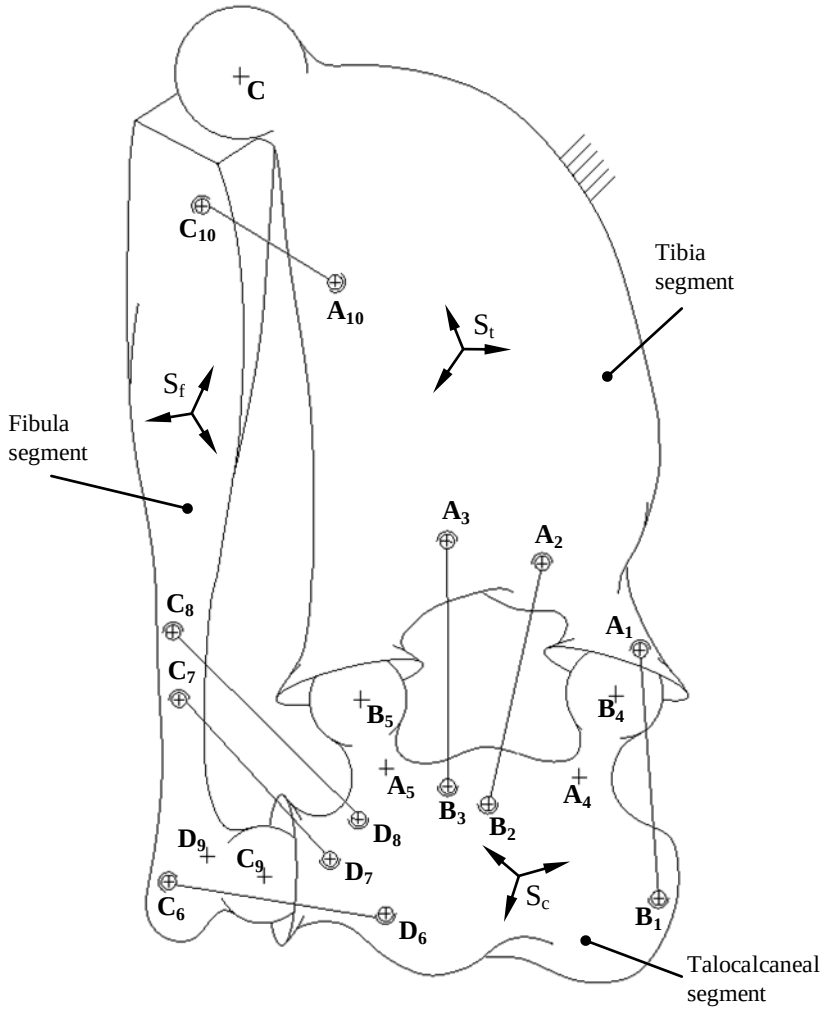


**Figure 4.4:** Synthetic schematic of the lower leg with **M3**.

TiCaL, CaFiL, ant-TaTiL, post-TaTiL, ant-TaFiL and post-TaFiL.

Based on these observations and assumptions, a more detailed schematic representation of the lower leg is shown in Figure 4.4, where every rigid link represents a specific anatomical element. Here the three talo/calcaneal, fibular and tibial segments feature three sphere-to-sphere contact points and one plane-to-sphere contact point, where points $A_i$ and $B_i$, $i$=4,5, represent the centres of the mating spherical surfaces fixed to the tibia and talus/calcaneus respectively and points $C_9$ and $D_9$ represent the centres of the mating spherical surfaces fixed to the fibula and talus/calcaneus respectively. Point $C$ represents the centre of the mating spherical surface fixed to the tibia. Moreover, points $A_i$ and $B_i$, $i$=1,2,3, represent the insertion points on the tibia and talus/calcaneus segments of the isometric fibre of the

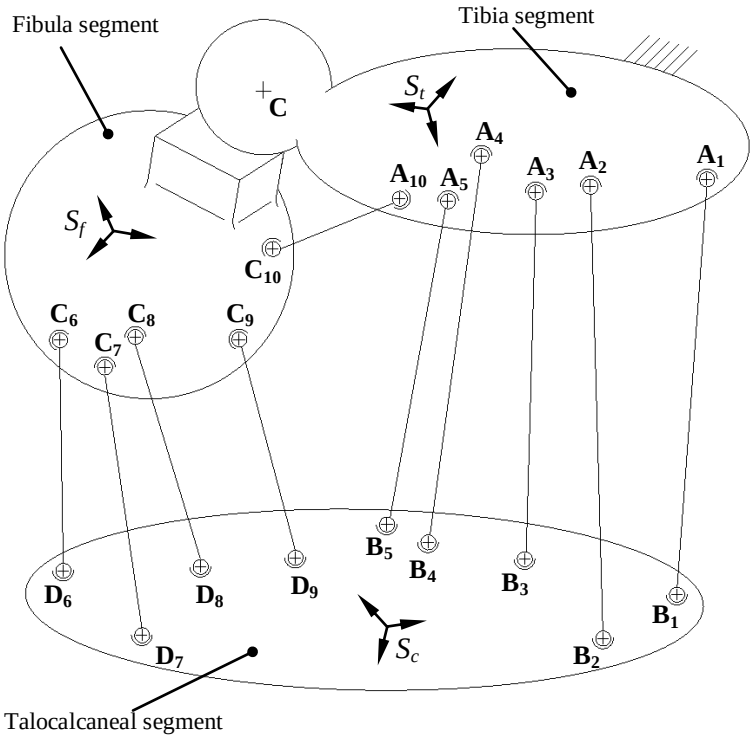


**Figure 4.5: M3** equivalent mehanism of the lower leg.

TiCaL, ant-TaTiL and post-TaTiL ligaments, points $C_j$ and $D_j$, $j$=6,7,8, represent the insertion points on the fibula and talus/calcaneus segments of the isometric fibre of the CaFiL ligament and of the ant-TaFiL and post-TaFiL ligaments. Points $C_{10}$ and $A_{10}$ represent the insertion points on the fibula and tibia segments of the interosseus membrane fibre.

Inspection of Figure 4.4, when considering, for instance, the tibia segment as a fixed body, and the ligament fibres as connected to the bones by spherical pairs centred at points $A_i$ and $B_i$, $i$=1,2,3, $C_j$ and $D_j$, $j$=6,7,8, and $C_{10}$ and $A_{10}$, reveals that the schematic represents a spatial mechanism with one-DOF. Indeed, Kutzbach's formula [52] provides one-DOF considering that the rotations of the ligaments about the respective axes $A_iB_i$, $i$=1,2,3, $C_jD_j$, $j$=6,7,8, and $C_{10}A_{10}$ are inessential to the relative position of the segments. In particular, the talo/calcaneal segment has a one-DOF motion with respect to the tibia segment because the two segments are constrained by two sphere-on-sphere high pairs and three rigid rods linked to the bone segments by spherical pairs: this means that the fibula segment is dragged by the relative motion between tibia and talus/calcaneus segments during the ankle passive flexion.

As already reported in chapter 2 and in section 4.1.1, during the relative motion of the three bone segments each pair of mating spherical surfaces can be represented by rigid rods with spherical pairs as ending

points which are the centres of the spheres. Based on this consideration, the equivalent mechanism of Figure 4.4 can be more synthetically represented by the mechanism shown in Figure 4.5. Here, the meaning of the points $A_i$, $i$=1,2,...,5, $A_{10}$, $C_j$, $j$=6,…,10, $B_i$, $i$=1,2,...,5, $D_j$, $j$=6,7,8,9, and $C$ is the same as in Figure 4.4. The elements $L_i = A_iB_i$, $i$=1,2,...,5, $L_j = C_jD_j$, $j$=6,7,8,9 and $L_{10} = A_{10}C_{10}$ can be regarded as constant length rigid links connected to two bone segments by spherical pairs centred at points $A_i$ and $B_i$, $i$=1,2,...,5, $C_j$ and $D_j$, $j$=6,7,8,9, and $A_{10}$ and $C_{10}$, respectively. As a result, the mechanism has one-DOF and in particular it provides the movable talo/calcaneal segment with one-DOF with respect to the tibia base (rotation of links about the axes defined by their ending points ($A_i$, $B_i$), ($C_j$, $D_j$) and ($A_{10}$, $C_{10}$) respectively is irrelevant to the relative mobility of the three main segments). In the following considerations, for the sake of simplicity, this latter mechanism will be considered as the equivalent mechanism of the lower leg.

### 4.2.2 The kinematic model

The mathematical model of the one-DOF equivalent mechanism shown in Figure 4.5, i.e. the model that provides the relationship between the independent variable of motion and the dependent ones, which define the configuration of the mechanism, is provided by the closure equations of the mechanism. The equations make it possible to find the relative position of the three bones (tibia, fibula and talus/calcaneus) during the ankle passive flexion. It is important to note that, with the relative position of the considered bones, the position of the other anatomical elements (such as for example the ligament insertion points) can also be easily found. In order to make the mathematical model (i.e., the equations) simpler than the one obtained based on the link-to-link Denavit-Hartenberg transformation matrices, the closure equations are provided using some kinematic constraints of the mechanism in a suitable way. In particular, in the equivalent mechanism shown in Figure 4.5, each rigid rod constrains the distance between the two rod ending points to not change during motion; moreover, the plane-to-sphere contact higher pair causes a specific constrained relative motion between the two segments in contact, namely the tibia and fibula (as will be shown below).

Actually, with reference to Figure 4.5, it can be noted that each pair of points ($A_i$, $B_i$), $i$=1,2,...,5, ($C_j$, $D_j$), $j$=6,7,8,9, and ($A_{10}$, $C_{10}$) is constrained to maintain a constant mutual distance $L_i$, $L_j$ and $L_{10}$ respectively during motion. This makes it possible to write:

$$\begin{aligned} &\| \mathbf{A}_i - R_{tc} \cdot \mathbf{B}_i - \mathbf{p}_{tc} \|^2 = L_i^2 \quad (i=1,\ldots,5) \\ &\| \mathbf{D}_j - R_{cf} \cdot \mathbf{C}_j - \mathbf{p}_{cf} \|^2 = L_j^2 \quad (j=6,\ldots,9) \\ &\| \mathbf{A}_{10} - R_{tf} \cdot \mathbf{C}_{10} - \mathbf{p}_{tf} \|^2 = L_{10}^2 \end{aligned} \tag{4.1}$$

where $\mathbf{A}_i$ is the position vector of the point $A_i$ measured in the reference system $S_t$ , $\mathbf{B}_i$ and $\mathbf{D}_j$ are respective the position vectors of the points $B_i$ and $D_j$ measured in the reference system $S_c$, and $\mathbf{C}_j$ is the position vector of the point $C_j$ measured in the reference system $S_f$. The Cartesian reference systems $S_t$, $S_c$ and $S_f$ are embedded in the tibia, talus/calcaneus and fibula segments respectively (see Figure 4.4 and Figure 4.5). The generic vector $\mathbf{p}_{ij}$ represents the position of the origin $O_j$ of the generic reference system $S_j$ with respect to the generic reference system $S_i$; the generic matrix $R_{ij}$ is the orthogonal rotation matrix 3x3 that transforms the components of a vector measured in the generic reference frame $S_j$ into the components of the same vector measured in the generic reference frame $S_i$ (the indices *c*, *t* and *f* refer to $S_c$, $S_t$ and $S_f$ reference systems respectively). The matrix $R_{ij}$ can be expressed as a function of three parameters that represent the orientation of the reference system $S_j$ with respect to $S_i$.

The plane-to-sphere articular contact between tibia and fibula in the proximal end can be represented by constraining the centre of the sphere to move on a plane parallel to the articulating plane that approximates the fibula surface in the proximal end (Figure 4.6). Hereafter, **n** denotes the unit vector perpendicular to the plane in contact with the sphere, *C* the centre of the sphere, *H* the point of the plane the point *C* belongs to. The plane-to-sphere contact is expressed as:

$$^t\mathbf{n} \cdot (\mathbf{C} - {}^t\mathbf{H}) = 0 \tag{4.2}$$

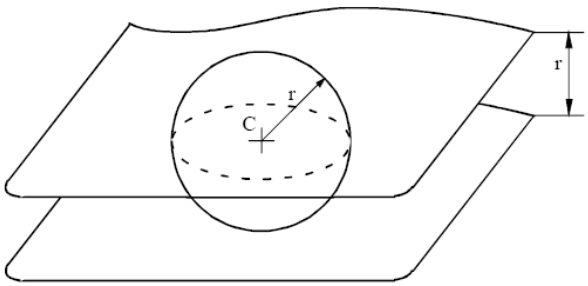


**Figure 4.6:** Plane-to-sphere contact.

with

$$\begin{aligned} {}^{t}\mathbf{n} &= R_{tf} \cdot \mathbf{n} \\ {}^{t}\mathbf{H} &= R_{tf} \cdot \mathbf{H} + \mathbf{p}_{tf} \end{aligned} \tag{4.3}$$

where the vector **n** is measured in the reference system $S_f$ , **H** is the position vector of the point *H* measured in the reference system $S_f$ , **C** is the position vector of the point *C* measured in the reference system $S_t$ , and the matrix $R_{tf}$ and the vector $\mathbf{p}_{tf}$ have the same meaning as explained above.

The system of equations (4.1) and (4.2) represents the closure equations of the mechanism. When considering the tibia as a fixed body, for a given geometry, this system can be regarded as a system of eleven nonlinear equations in twelve variables, that are the three components of vector $\mathbf{p}_{tf}$, the three orientation parameters that define the rotation matrix $R_{tf}$, the three components of vector $\mathbf{p}_{tc}$ and the three orientation parameters that define the rotation matrix $R_{tc}$. Given the angle that measures the ankle flexion - i.e. the rotation between talus and tibia in the saggital plane -, the remaining eleven variables can be found by solving the system of equations (4.1) and (4.2). Then, by simple matrix operations, the position vector $\mathbf{p}_{cf}$ and the matrix $R_{cf}$ can be easy calculated using the vectors $\mathbf{p}_{tf}$ and $\mathbf{p}_{tc}$, and the matrices $R_{tf}$ and $R_{tc}$. For instance, if ${}^{t}\mathbf{x}$ is a vector measured in the reference system $S_t$, it can be written:

$${}^{t}\mathbf{x} = R_{tf} \cdot {}^{f}\mathbf{x} + \mathbf{p}_{tf} \tag{4.4}$$

$${}^{t}\mathbf{x} = R_{tc} \cdot {}^{c}\mathbf{x} + \mathbf{p}_{tc} \tag{4.5}$$

where ${}^{f}\mathbf{x}$ and ${}^{c}\mathbf{x}$ represent the vector ${}^{t}\mathbf{x}$ measured in the reference system $S_f$ and $S_c$ respectively. Thus, by means of equation (4.5), ${}^{c}\mathbf{x}$ can be obtained as:

$${}^{c}\mathbf{x} = \mathrm{inv}(R_{tc}) \cdot ({}^{t}\mathbf{x} - \mathbf{p}_{tc}) \tag{4.6}$$

and introducing equation (4.4) in equation (4.6):

$$\begin{aligned} {}^{c}\mathbf{x} &= \mathrm{inv}(R_{tc}) \cdot (R_{tf} \cdot {}^{f}\mathbf{x} + \mathbf{p}_{tf} - \mathbf{p}_{tc}) = \\ &= \mathrm{inv}(R_{tc}) \cdot R_{tf} \cdot {}^{f}\mathbf{x} + \mathrm{inv}(R_{tc}) \cdot (\mathbf{p}_{tf} - \mathbf{p}_{tc}) \end{aligned} \tag{4.7}$$

By inspection on equation (4.7), the vector $\mathbf{p}_{cf}$ and the matrices $R_{cf}$ can be easily deduced:

$$\begin{aligned} \mathbf{p}_{cf} &= \text{inv}(R_{tc}) \cdot (\mathbf{p}_{tf} - \mathbf{p}_{tc}) \\ R_{cf} &= \text{inv}(R_{tc}) \cdot R_{tf} \end{aligned} \tag{4.8}$$

### 4.2.3 The synthesis

The procedure to synthesize the optimal equivalent mechanism needs anatomical data which are fundamental to define the geometry of the mechanism. Thus, experimental sessions are necessary to measure both the main elements of the anatomical structures (as articular surfaces and insertion areas of ligaments) and the passive motion of the tibia, fibula and talus bones during the ankle passive flexion.

In order to describe the relative position and rotation of the bones, the anatomical frames embedded respectively in the tibia, the fibula and talo/calcaneal segments are defined and a sequence-independent joint coordinate system is chosen (as explained in the next section 4.2.4).

The geometry of the equivalent mechanism (Figure 4.5) is defined by 78 parameters: namely, $3 \cdot 20 = 60$ coordinates of the centres of the spherical pairs, ten link lengths $L_i$, $i$=1,2,...,10, two directional cosines that define the unit vector **n** perpendicular to the plane, three coordinates of the centres $C$ of the sphere that approximates the tibia surface at the proximal end, three coordinates of the point $H$ that belongs to the plane the point $C$ belongs to.

In order to find the optimal set of parameters and the related mechanism which allows the best simulation of the lower leg experimental passive motion, the procedure already presented in [11] is adopted. This procedure starts from a first tentative geometry of the mechanism that is defined using the measurement of the main anatomical structures of the lower leg. The geometric parameters of the mechanism are then refined with an iterative process based on an error function $f$ (objective function) that compares the poses of the movable bone segments - the fibula and the talus/calcaneus segments - obtained by the kinematic analysis of the mechanism, with the poses obtained by measurement data. In particular, the error function, which is computed at each step of iteration, is the sum of the weighted errors of the experimental values with respect to the calculated values, for the $n$ values of the ankle flexion angle considered:

$$f = \sum_{j=1}^{11} \sum_{i=1}^{n} \frac{(x_{ji} - x^*_{ji})^2}{(x_{j\max} - x^*_{j\min})^2} \tag{4.9}$$

where, $x_{ji}$ is the actual value of the j-th dependent variable, $j$=1,…,11, at the $i$-th pose, $i$=1, …,$n$; $x^*_{ji}$ is the corresponding experimental value of the variable $xji$; $x_{jmax}$ and $x_{jmin}$ are the maximum and the minimum values of each of the dependent variables at the end of the process. If closure equation system (4.1) and (4.2) does not provide a real solution for all the $n$ configurations considered, then the objective function $f$ cannot be computed and it is given an arbitrarily high value. Since $f$ is highly nonlinear and has discontinuities, the most traditional optimization methods, based on the gradient or on higher derivatives of the objective function and used to search for a relative minimum, do not provide good solutions to this problem. In the different approach proposed here, the optimization problem is initially solved by means of a genetic algorithm. In particular, the "ga" function of Matlab can be used in order to find a minimum of $f$; because the genetic algorithm may converge towards a local optimal solution rather than towards the global optimum of the problem, it is recommended to repeat the optimization procedure several times and then to refine the best obtained solution by means of a quasi-Newtonian algorithm.

It is worth introducing lower and upper bounds on the values of the 78 parameters, so that the points $A_i$, $i$=1,2,...,5, $A_{10}$, $C_j$, $j$=6,7,8,9, $C_{10}$, $B_i$, $i$=1,2,...,5, $D_j$, $j$=6,7,8,9, $C$ and $H$, and the unit vector **n**, that define the geometry of the equivalent mechanism, provide a final geometry of the optimized equivalent mechanism which retains the anatomical feature of the lower leg (a more in-depth description of the optimization procedure is in Appendix).

### 4.2.4 Case study: comparison between simulation and experimental results

In order to obtain the physical data necessary to synthesize the equivalent mechanism of the lower leg, data from previous experimental sessions were used. With the experimental procedure shown in [11,13], the talocrural joint articular surfaces and the insertion areas of the CaFiL and TiCaL ligaments were obtained; the desired passive motion of the talus and the fibula with respect to the tibia were also measured. In particular, the poses of the trackers fixed to the tibia, the fibula and the talus respectively were measured with respect to a Cartesian reference system fixed to the camera system used as acquisition system, while the coordinates of points measured by a pointer were given in the reference systems of the trackers. The

anatomical data not provided by previous experiments - i.e., the insertion areas of ant-TaTiL, post-TaTiL, ant-TaFiL and post-TaFiL ligaments and of the interosseus membrane fibres, and the articular surfaces of tibia and fibula in the upper extremity – were taken from the literature. In particular, the surfaces of tibia, fibula and talus bones taken from literature were scaled in a homogeneous way along the three Cartesian axes, in order to fit the talocrural joint articular surfaces digitized in the previous experimental session (the procedure is the same depicted in Figure 3.4); thus, the tibia and fibula articular surfaces at their proximal end were obtained. Then the ligament insertions were found on the obtained bone surfaces, using anatomical images and data.

The tibia anatomical frame ($S_t$) and the talus anatomical frame ($S_c$) were defined using some well-recognizible anatomical points. In particular, $S_c$ was found as it described in section 3.4. Instead, $S_t$ was found using the tibial reference pints MM and TT (see Figure 3.8a) and the fibular reference points LM and HF (see Figure 3.8b) when the ankle joint is in neutral position (as defined by the International Society of Biomechanics [53]); the definition of $S_t$ is the same that is described in section 3.4 for the tibia/fibula anatomical frame. The absence of many experimental anatomical data of the fibula bone made it impossible to define an anatomical frame embedded in the fibula; the reference frame of the tracker fixed to the fibula bone was thus considered as the reference frame $S_f$.

A sequence-independent joint coordinate system [30] was adopted in order to describe the orientation of the talus with respect to the tibia. The three following rotation axes were chosen: the $z_t$ axis of $S_t$ fixed to the tibia as the first one, the $y_c$ axis of $S_c$ fixed to the talus as the second one, finally an axis coincident with the shortest distance straight line of the other two axes as the third one. Three angles about these axes were defined: the ankle dorsiflexion(+)/plantarflexion(-) angle $\gamma$ about the z-axis of $S_t$, the ankle internal(+)/external(-) rotation angle $\alpha$ about the y-axis of $S_c$, and the ankle pronation(+)/supination(-) angle $\beta$ about a floating axis defined by the cross vector product of the unit vectors of the z-axis of $S_t$ and the unit vector of the y-axis of $S_c$. Based on this convention, the rotation matrix $R_{ct}$ was obtained, which can be represented by an expression similar to (3.6).

The joint coordinate system that defines the orientation of the fibula with respect to the tibia was chosen in the same way as the one of the talus with respect to the tibia. Likewise, the matrix $R_{ft}$ can be expressed by (3.6).

Based on experimental and literature data, a first tentative geometry of the mechanism was then defined. In particular, for the generation of the kinematic pairs modelling the articular contacts at the ankle joint the following approach was used: the areas of the surfaces of the mating bones which come into contact during the passive motion and which were previously digitalized were approximated by their best fit spherical surfaces. With the same approach, the tibia and fibula articular surfaces at their

proximal end, which were found from literature data, were approximated by their best fit spherical and planar surfaces respectively in order to model the articular contact between the two bones (Figure 4.3). The objective function of the iterative process that provides the optimal geometry of the mechanism was used only for the poses of the talus/calcaneus segment with respect to the tibia one because the poses of the tracker embedded in the fibula are believed to be not significant in analysing the fibula motion. However, during ankle passive flexion, the fibula segment motion was limited to prevent non anatomical displacements. In particular, the point $C_9$, that represents the centre of the sphere that approximates the contact surface of the fibula in the lateral malleolus, was constrained to move inside a small

| | **x [mm]** | **y [mm]** | **z [mm]** | **lenght [mm]** |
|---|---|---|---|---|
| $A_1$ | 1,229 | 13,886 | 36,510 | - |
| $A_2$ | 1,595 | 21,155 | 28,081 | - |
| $A_3$ | 3,949 | 15,083 | 33,483 | - |
| $A_4$ | 4,182 | 7,767 | 11,833 | - |
| $A_5$ | 12,559 | -4,195 | -3,714 | - |
| $A_{10}$ | 13,013 | 103,580 | -18,510 | - |
| $B_1$ | -14,209 | -21,473 | 29,893 | - |
| $B_2$ | 7,881 | -21,839 | 10,398 | - |
| $B_3$ | -26,293 | -23,727 | 30,431 | - |
| $B_4$ | -14,086 | -14,815 | 9,891 | - |
| $B_5$ | -11,713 | -14,214 | -3,319 | - |
| $D_6$ | -47,171 | -38,379 | -7,024 | - |
| $D_7$ | -7,715 | -15,388 | -14,858 | - |
| $D_8$ | -87,580 | 19,810 | 30,818 | - |
| $D_9$ | -22,168 | -17,236 | -47,669 | - |
| $C_6$ | -30,924 | 159,340 | -9,505 | - |
| $C_7$ | -16,073 | 138,230 | 1,343 | - |
| $C_8$ | -24,561 | 148,130 | -21,234 | - |
| $C_9$ | -51,610 | 129,630 | -0,989 | - |
| $C_{10}$ | -11,765 | 40,672 | -16,166 | - |
| $H$ | 8,719 | -187,040 | -11,502 | - |
| **n** | -0,261 | 0,042 | - | - |
| $C$ | 16,276 | 341,900 | -49,551 | - |
| $L_1$ | - | - | - | 25,980 |
| $L_2$ | - | - | - | 32,668 |
| $L_3$ | - | - | - | 35,141 |
| $L_4$ | - | - | - | 8,927 |
| $L_5$ | - | - | - | 10,591 |
| $L_6$ | - | - | - | 35,372 |
| $L_7$ | - | - | - | 14,490 |
| $L_8$ | - | - | - | 87,384 |
| $L_9$ | - | - | - | 15,162 |
| $L_{10}$ | - | - | - | 15,112 |

**Table 4.1:** Geometrical data of the mechanism obtained by the optimization procedure.

| | x [mm] | | y [mm] | | z [mm] | | lenght [mm] | |
|---|---|---|---|---|---|---|---|---|
| | first | opt | first | opt | first | opt | first | opt |
| *TiCaL* | | | | | | | | |
| $A_1$ | -1,445 | 1,229 | 15,152 | 13,886 | 34,749 | 36,510 | - | - |
| $B_1$ | -12,837 | -14,209 | -21,951 | -21,473 | 31,122 | 29,893 | - | - |
| $L_1$ | - | - | - | - | - | - | 26,772 | 25,980 |
| *ant-TaTiL* | | | | | | | | |
| $A_2$ | 10,264 | 1,595 | 21,115 | 21,155 | 26,611 | 28,081 | - | - |
| $B_2$ | 0,974 | -7,881 | -22,427 | -21,839 | 10,778 | 10,398 | - | - |
| $L_2$ | - | - | - | - | - | - | 31,176 | 32,668 |
| *post-TaTiL* | | | | | | | | |
| $A_3$ | 0,141 | 3,949 | 16,198 | 15,083 | 31,073 | 33,483 | - | - |
| $B_3$ | -26,226 | -26,293 | -24,744 | -23,727 | 23,300 | 30,431 | - | - |
| $L_3$ | - | - | - | - | - | - | 34,616 | 35,141 |
| *CaFiL* | | | | | | | | |
| $C_6$ | -29,786 | -30,924 | 158,120 | 159,340 | -8,682 | -9,505 | - | - |
| $D_6$ | -47,755 | -47,171 | -39,348 | -38,379 | -7,689 | -7,024 | - | - |
| $L_6$ | - | - | - | - | - | - | 34,547 | 35,372 |
| *ant-TaFiL* | | | | | | | | |
| $C_7$ | -18,139 | -16,073 | 137,900 | 138,230 | 1,859 | 1,343 | - | - |
| $D_7$ | -8,244 | -7,715 | -17,182 | -15,388 | -15,256 | -14,858 | - | - |
| $L_7$ | - | - | - | - | - | - | 12,780 | 14,490 |
| *post-TaFiL* | | | | | | | | |
| $C_8$ | -25,211 | -24,561 | 146,860 | 148,130 | -20,068 | -21,234 | - | - |
| $D_8$ | -87,920 | -87,580 | 20,721 | 19,810 | 30,214 | 30,818 | - | - |
| $L_8$ | - | - | - | - | - | - | 87,138 | 87,384 |
| *interosseus membrane fibre* | | | | | | | | |
| $A_{10}$ | 11,653 | 13,013 | 105,600 | 103,580 | -16,908 | -18,510 | - | - |
| $C_{10}$ | -12,151 | -11,765 | 40,958 | 40,672 | -17,059 | -16,166 | - | - |
| $L_{10}$ | - | - | - | - | - | - | 17,792 | 15,112 |

**Table 4.2:** Comparison between geometrical data of the links that model ligaments in the first tentative mechanism (first) and the optimized mechanism (opt).

volume which was defined by analysing the relative motion between fibula and tibia bones [35-41]. In particular, the limit for the range of motion of point $C_9$ along the $x$, $y$ and $z$ axis of $S_t$ was set at 1.5, 1.5 and 4 mm respectively.

The geometry of the equivalent mechanism obtained by the optimization procedure is reported in Table 4.1. The distance between corresponding points in the initial mechanism and in the final mechanism is generally very low, about 1-9 mm for the ligament insertions, and about 2-11

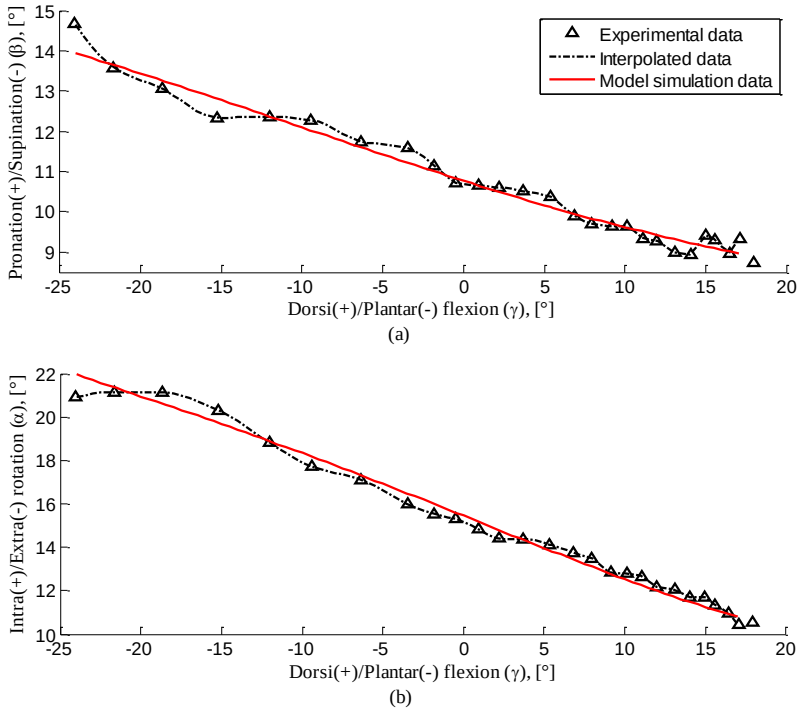


**Figure 4.7:** Passive motion simulation of the talus/calcaneus respect to the tibia: angles β, (a), and α (b) versus ankle's flexion angle γ.

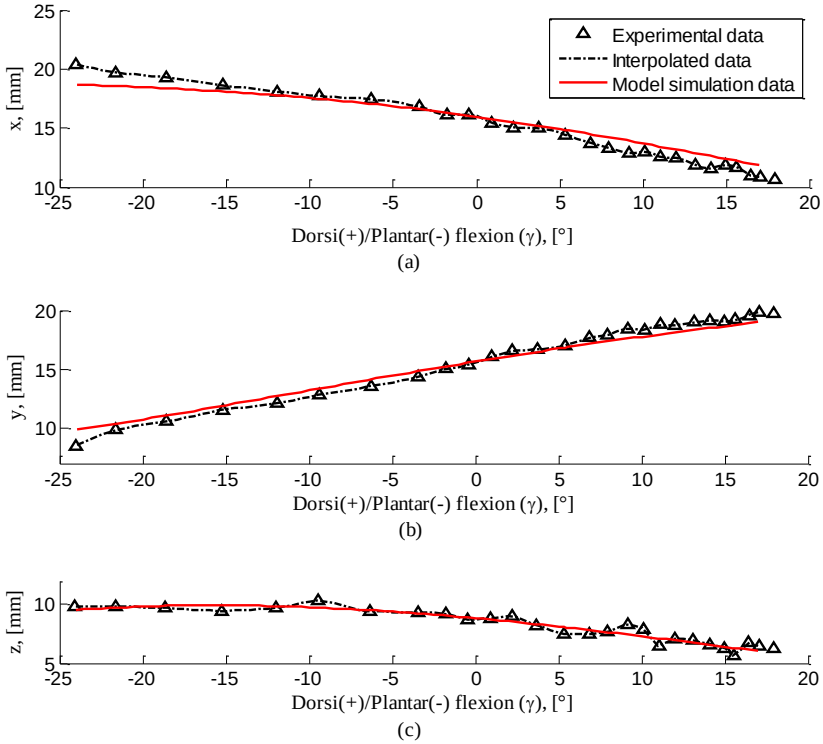


**Figure 4.8:** Passive motion simulation of the talus/calcaneus respect to the tibia: x, (a), y, (b), and z, (c), versus ankle's flexion angle γ.

mm for the centres of the sphere. In particular, in Table 4.2 the comparison between the anatomical data of ligaments and the geometrical data of links modeling ligaments in the optimized mechanism is reported.

The results of the ankle passive motion simulation (the relative passive motion between talo/calcaneal and tibia segments) obtained by the model (equivalent mechanism) were compared with those obtained by measurements. In particular, Figure 4.7 and Figure 4.8 show the angles $\alpha$ and $\beta$, and the positions x, y, and z of the origin of the reference system $S_c$ with respect to $S_t$, respectively versus the ankle flexion angle $\gamma$. All figures show both the simulation and the experimental results. In particular, the experimental results are identified by the symbol $\Delta$ and interpolated by a dotted line. The interpolation makes it possible to use a higher number of (interpolated) experimental data, which may be useful for the optimal synthesis of the equivalent mechanism geometry. Inspection of the figures shows that the new equivalent spatial mechanism replicates the passive motion of the human ankle quite well.

It is worth noting that different geometries of the equivalent mechanism could have been synthesized which might better fit the experimental data of the passive motion, but their geometry may not fit the anatomical structures of the natural lower leg well. The geometry synthesized in this paper and reported in Table 4.1 is the best compromise that can well fit both the lower leg passive motion and the lower leg's main anatomical structures.

In conclusion, although incomplete experimental data were used, the results show the efficiency of the proposed new mechanism to simulate the lower leg passive motion and, at the same time, the potentiality of the mechanism to replicate the main anatomical structures quite well. Moreover, by involving different anatomical structures that affect the ankle kinematic behavior, the presented model can play an important role for future development of a model that will describe the motion of the whole lower leg, in passive condition or in response to external loads.

Further experimental works are necessary in order to validate the potential of the proposed model with a higher number of specimens.

# Chapter 5

# Conclusion

Mathematical models of human joints are important tools which have both theoretical and practical applications. They can be used by researchers to fully understand the stabilizing role of the components of the joint, by engineers as an aid for prosthetic design, by surgeons during the planning of an operation or during the operation itself, and last, but not least, by orthopedists for diagnosis and rehabilitation purposes.

As regards the ankle complex joint, the lack of interpreting models and the poor results of total ankle replacement arthroplasty have strongly suggested devising new mathematical models capable of reproducing the restraining function of each structure of the joint and of replicating the relative motion of the bones which constitute the joint itself. It is clear that the first point is functional to the second one.

An important contribution has been given by some researches who have proposed a new approach which allows the replication of both the kinematic behaviour and the anatomical geometry of the ankle complex. The approach relies upon rigid link mechanisms whose members represent determinate components of the joint. These mechanisms showed to be able to simulate the passive motion of the ankle complex with good accuracy maintaining their geometry close to the anatomy.

The first goal reached by this work is the developing of new models of the ankle complex which allow the investigation on the role of all the main ligaments of the joint. In particular, nine 5-5 FPMs have been synthesized for the simulation of the ankle passive motion; each mechanism takes into consideration two among all the ligaments. The nine models have been identified from experimental data by means of optimization procedure. Then, the simulated motions obtained by the models have been compared to the experimental one. Each mechanism (except for one) accurately reproduce the kinematic behaviour of the joint under virtually unloaded conditions, showing that ankle ligaments can be considered as redundant constraints during passive motion.

Moreover, a new one-DOF spatial mechanism is developed for modelling the passive motion of the lower leg in which the ankle complex plays a fundamental role. The model considers many passive structures that constitute the articulation, overcoming the limitations of previous models which took into account only few anatomical elements of the ankle

complex. The mechanism has been defined with experimental measurement and then refined by an optimization procedure. The comparison between simulation results and experimental data shows that the proposed mechanism can replicate the relative motion of the bones which constitute the ankle complex with the same accuracy of the previous simple models.

In conclusion, the new mechanisms for the ankle complex passive motion simulation proved to be successful and thus promising for the definition of more complex models which could also involve the elasticity of passive structures, the effect of muscular forces and external loads.

# Appendix

# The optimization procedure

The preliminary estimate of the geometrical parameters is only a rough approximation of the final model: in order to best-fit the experimental results, these parameters have to be optimized.

The optimization technique applied to the mechanisms is represented in Figure A.1. The first guess $\mathbf{q_0}$ is passed to an objective function. The model is defined within the function, by means of $\mathbf{q_0}$. The passive motions of the joint are obtained by solving the closure equations at the given flexion angles; the simulated motions **x** are then compared to the experimental ones **x*** and the differences are quantified by an objective function *f*. The value of this index leads the optimization algorithm to define a second guess $\mathbf{q_1}$ (compatible with the bounds) which is passed again to the objective function. The iteration is repeated until the minimum value of *f* is reached. The final parameter set $\mathbf{q_f}$ is the solution of the optimization problem.

In particular, the poses of the movable bone segments computed from the model are iteratively compared with the experimental ones: the sum of the weighted squares of errors between the poses constitutes the objective function *f* which has to be minimized. If $x_{ji}$ is the computed value of the *j*-th, j=1,...,*k*, dependent variable of the closure equations of the mechanism, obtained at the *i*-th flexion angle, *i*=1,...,*n*, the contribution of $x_{ji}$ to the value of *f* is:

$$f_{ij} = \frac{(x_{ji} - x^*_{ji})^2}{x^2_{jd}} \qquad \text{(A.1)}$$

where $x^*_{ji}$ is the corresponding experimental value. The weights $x_{jd}$ are necessary, since the unknowns have different physical dimensions (some are angles, others are lengths). The weights only depend on the unknown and are chosen as:

$$x_{jd} = \max\{x_{jd}, i = 1,...,k\} - \min\{x_{jd}, i = 1,...,k\} \qquad \text{(A.2)}$$

APPENDIX

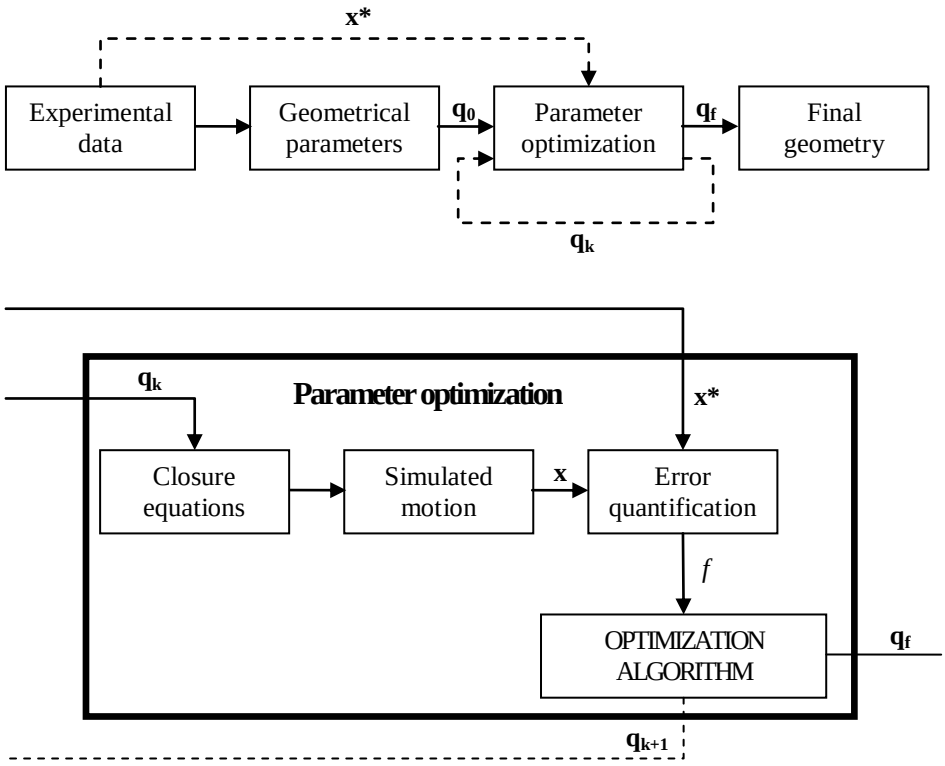


**Figure A.1:** The optimization procedure for the identification of the passive motion model

Thus, the error $f_{ji}$ is a sort of per cent error, with respect to the maximum range $x_{jd}$ of the $j$-th pose parameter.

The mechanism closure is not guaranteed for every parameter set: if the model closures are not satisfied at all the given flexion angles, an arbitrary high value is assigned to the index $f$. Thus, the complete algorithm for the computation of $f$ is:

$$\begin{aligned} f &= \sum_{j=1}^{k}\sum_{i=1}^{n} f_{ij} && \text{if closure succeeds} \\ f &= X && \text{otherwise} \end{aligned} \qquad \text{(A.3)}$$

where $X$ is an arbitrary high value. As previously noted, in order to give the proposed model a physical consistency, the optimization research domain is bounded, having the starting guess as the central value: every parameter $q_m$ has to fall within the interval $[q_{0m}-\delta_m, q_{0m}+\delta_m]$.

The objective function is highly non-linear and, because of the bifurcation of (A.3), it presents many discontinuities. Quasi-Newton

methods are powerful optimization algorithms which can efficiently find the minimum value of non-linear functions; unfortunately — like all deterministic algorithms which make use of derivatives of the objective function — they show numerical instabilities when solving discontinuous problems. Thus, a first approximation of the optimum solution is found by means of a heuristic algorithm, i.e. a genetic algorithm, which does not make use of derivatives. The bounded genetic algorithm makes it possible to find a feasible solution within the bounds. The preliminary solution is then iteratively refined by means of a quasi-Newton algorithm: the search for the optimum solution is carried out by "guiding" the minimum on even bigger domains inside the bounds and by keeping the algorithm on continuous zone of the objective function.

APPENDIX

# Bibliography


[1] A. Erdemir, S. McLean, W. Herzog, and A.J. van den Bogert, 2006. "Model-based estimation of muscle forces exerted during movements". *Clinical Biomechanics*, 22(2), pp. 131–154.

[2] Z. Ji, T. Findley, H. Chaudhry, and B. Bruce, 2004. "Computational method to evaluate ankle postural stiffness with ground reaction forces". *Journal of Rehabilitation Research and Development*, 41, pp. 207–214.

[3] R.B. Pilkar, J.C. Moosbrugger, V.V. Bhatkar, R.J. Schilling, C.M. Storey and C.J. Robinson, 2007. "A biomechanical model of human ankle angle changes arising from short peri-threshold anterior translations of platform on which a subject stands". In *29th Annual International Conference of IEEE-EMBS*, pp. 4308–4311.

[4] A.H. Hansen, D.S. Childress, S.C. Miff, S.A. Gard and K.P. Mesplay, 2004. "The human ankle during walking: implications for design of biomimetic ankle prostheses". *Journal of Biomechanics*, 37, pp. 1467–1474.

[5] H.M. Schepers and P.H. Veltink, 2006. "Estimation of ankle moment using ambulatory measurement of ground reaction force and movement of foot and ankle". In *First IEEE/RAS-EMBS International Conference on Biomedical Robotics and Biomechatronics*, pp. 399–401.

[6] H.M. Schepers, H. Koopman and P.H. Veltink, 2007. "Ambulatory assessment of ankle and foot dynamics". In *IEEE Transactions on Biomedical Engineering*, pp. 895–902.

[7] A. Leardini, J.J. O'Connor, F. Catani, and S. Giannini, S., 1999. "A geometric model of the human ankle joint". *Journal of Biomechanics*, 32(6), pp. 585–591.

[8] F. Corazzaa, J.J. O'Connor, A. Leardini, V. Parenti Castelli, 2003. "Ligament fibre recruitment and forces for the anterior drawer test at the human ankle joint". *Journal of Biomechanics*, 36, pp. 363–372.

[9] R. Di Gregorio, V. Parenti-Castelli, J.J. O'Connor, and A. Leardini, 2004. "Equivalent spatial parallel mechanisms for the modelling of the ankle passive motion". In *Proceedings of the ASME Design Engineering Technical Conference*, 2, pp. 679–688. DETC2004-57251.

BIBLIOGRAPHY


[10] R. Di Gregorio, R., V. Parenti-Castelli, J.J. O'Connor and A. Leardini, 2007. "Mathematical models of passive motion at the human ankle joint by equivalent spatial parallel mechanisms", *Medical & Biology Engineering & Computing*, 45(3), pp. 305–313.

[11] R. Franci, and V. Parenti-Castelli, 2007. "A 5-5 one-degree-of freedom fully parallel mechanism for the modeling of passive motion at the human ankle joint". In *Proceedings of ASME-IDETC/CIE 2007, International Design Engineering Technical Conferences and Computers and Information in Engineering, Las Vegas, Nevada, USA, September, 4–7*, pp. 1–8.

[12] R. Franci, and V. Parenti-Castelli, 2008. "A one-degree-of-freedom wrist for the modelling of passive motion of the human ankle joint". In *Proceedings of IAK 2008, Conference of Interdisciplinary Applications of Kinamatic, Lima, Per, USA, January, 9–11*, pp. 1–13.

[13] R. Franci, V. Parenti-Castelli, C. Belvedere, and A. Leardini, 2009. "A new one-DOF fully parallel mechanism for modelling passive motion at the human tibiotalar joint". *Journal of Biomechanics*, 42(10): pp. 1403–1408.

[14] Primal Pictures. *Primal 3D Interactive series: ankle.* Primal Pictures Ltd, 2003.

[15] H. Gray, 1918. "Anatomy of the Human Body*"*. Philadelphia : Lea & Febiger ed.

[16] B. Baldisserri and V. Parenti Castelli, 2011. "Passive motion modeling of the human ankle complex joint". In *Proceedings of IFToMM 2011, 13th World Congress in Mechanism and Machine Science*.

[17] J.W. Goodfellow, and J.J. O'Connor, 1978. "The mechanics of the knee and prosthesis design". *Journal of Bone Joint Surgery [Br]*, 60-B, pp. 358–369.

[18] L. Blankevoort, R. Huiskes, and A.D. Lange, 1988. "Envelope of passive knee joint motion". *Journal of Biomechanics*, 21(9), pp. 705–720.

[19] D. Wilson, and J.J. O'Connor, 1997. "A three-dimensional geometric model of the knee for the study of joint forces in gait". *Gait and Posture*, 5, pp. 108–115.

[20] A. Leardini, J.J. O'Connor, F. Catani, and S. Giannini, S., 1999. "Kinematics of the human ankle complex in passive flexion: a single degree of freedom system". *Journal of Biomechanics*, 32(2), February, pp. 111–118.

[21] C. Saltzman, T. McIff, J. Buckwalter, T.D. Brown, 2000. "Total ankle replacement revisited". *J. Orthop. Sports Phys. Ther.*, 30(2), pp. 56–67.

[22] B. Hintermann, and V. Valderrabano, 2003. "Total ankle replacement". *Foot Ankle Clin*., 8, pp. 375–405.

[23] H. Zwipp, S. Rammelt, and R. Grass, 2002. "Ligamentous injuries about the ankle and subtalar joints". *Clin. Podiatr. Med. Surg*., 19(2), pp. 195–229.

[24] G. Kerkhoffs, P. Struijs, R. Marti, L. Blankevoort, W. Assendelft, C.V. Dijk, 2003. "Functional treatments for acute ruptures of the lateral ankle ligament: a systematic review". *Acta Orthop. Scand.*, 74(1), pp. 69–77.

[25] V. Parenti-Castelli, and R. Di Gregorio, 2000. "Parallel mechanisms applied to the human knee passive motion simulation". In *Advances in Robot Kinematics, J. Lenarcic and M. S. Eds., eds. Kluwer Academic Publisher*, pp. 333–344. ISBN 0-7923-6426-0.

[26] R. Di Gregorio, and V. Parenti-Castelli, 2003. "A spatial mechanism with higher pairs for modelling the human knee joint". *Journal of Biomechanical Engineering*, 125(2), pp. 232–237.

[27] N. Sancisi and V. Parenti-Castelli, 2007. "A 1-dof parallel spherical wrist for the modelling of the knee passive motion". In *Proceedings of IFToMM 2007, Besanc¸on, France, June 17–21*, pp. 1–6.

[28] N. Sancisi and V. Parenti-Castelli, 2010. "A new kinematic model of the passive motion of the knee inclusive of the patella". *Mechanism and Machine Theory*, 45(4), pp. 658–665.

[29] N. Sancisi and V. Parenti-Castelli, 2011. "A novel 3D parallel mechanism for the passive motion simulation of the patella-femur-tibia complex". *Meccanica*, 46(1), pp. 207–220.

[30] E. Grood, and W. Suntay, 1983. "A joint coordinate system for the clinical description of three-dimensional motions: application to the knee". *Journal of Biomechanical Engineering*, 105 (2), pp. 136–144.

[31] B. Baldisserri and V. Parenti Castelli, 2009. "A preliminary study for a kinematic model of the complex tibia-fibula-talus-calcaneus". In *Giornata di studio in onore di Ettore Funaioli 2009*, Asterisco edizioni, pp. 325–340.

[32] B. Baldisserri and V. Parenti Castelli, 2010. "A new spatial kinematic model of the lower leg complex: a preliminary study". In *Proceedings of EUCOMES 2010, 3-rd European Conference on Mechanism*

*Science, Cluj-Napoca, Romania, September 14-18, 2010*, pp. 295–302.

[33] B. Baldisserri and V. Parenti Castelli. "A new 3D kinematic model for the passive motion of the tibia-fibula-ankle complex." In *Proceedings of ASME-IDETC/CIE 2010, International Design Engineering Technical Conferences and Computers and Information in Engineering Conference, Montreal, Quebec, Canada, August 15-18, 2010*.

[34] B. Baldisserri and V. Parenti Castelli, 2012. "A new 3D mechanism for modeling the passive motion of the tibia-fibula-ankle complex". *Journal of Mechanisms and Robotics*, in press.

[35] J. Kärrholm, L.I. Hansson and G. Selvik, 1985. "Mobility of the lateral malleolus, a roentgen stereophotogrammetric analysis". *Acta Orthopedica Scandinavica*, 56, pp. 479–483.

[36] T. Ahl, N. Dalen, A. Lunberg and G. Selvik, 1987. "Mobility of the ankle mortise, a roentgen stereophotogrammetric analysis". *Acta Orthopedica Scandinavica*, 58, pp. 401–402.

[37] O.K. Svensson, A. Lunberg, G. Walheim and G. Selvik, 1989. "*In vivo* fibular motions during various movements of the ankle". *Clinical Biomecnics*, 4, pp. 155–160.

[38] A. Beumer, E.R. Valstar, E.H. Garling, R. Niesing, J. Ranstam, R. Löfvenberg and B.A. Swierstra, 2003. "Kinematics of the distal tibiofibular syndesmosis. Radiostereometry in 11 normal ankles". *Acta Orthopedica Scandinavica*, 74, pp. 337–343.

[39] L. Bragonzoni, A. Russo, M. Girolami, U. Albisinni, A. Visani, N. Mazzotti, and M. Marcacci, 2006. "The distal tibiofibular syndesmosis during passive foot flexion. RSA-based study on intact, ligament injured and screw fixed cadaver specimens". *Arch Orthop Trauma Surg*, 126, pp. 304–308.

[40] A. Arndt, P. Wolf, A. Liu, C. Nester, A. Stacoff, R. Jones, P. Lundgren, and A. Lundberg, 2007. "Intrinsic foot kinematics measured in vivo during the stance phase of slow running". Journal of Biomechanics, 40, pp., 2672–2678.

[41] M. Bozkurt, E. Tonuk, A. Elhan, I. Tekdemir, M.N. Doral, 2008. "Axial Rotation and Madiolateral Translation of the Fibula during Passive Plantarflexion". *Foot & Ankle International*, 29, pp. 502–507.

[42] P.C. Liacouras and J.S. Wayne, 2007. "Computational modeling to predict mechanical function of joints: application to the lower leg with simulation of two cadaver studies". *Journal of Biomechanical Engineering*, 129, pp. 811–817.

[43] B. Koopman, H.J. Grootenboer and H.J. de Jongh, 1995. "Inverse dynamics model for the analysis, reconstruction and prediction of bipedal walking". *Journal of Biomechanics*, 28(11), pp. 1369–1376.

[44] U. Glitsch and W.S. Baumann, 1997. "Three-dimensional determination of internal loads in the lower extremity". *Journal of Biomechanics*, 30(11-12), pp. 1123–1131.

[45] R. Neptune, S. Kautz and F. Zajac, 2001. "Contributions of the individual ankle plantar flexors to support, forward progression and swing initiation during walking". *Journal of Biomechanics*, 34(11), pp. 1387–1398.

[46] M. Gunther and R. Blickhan, 2002. "Joint stiffness of the ankle and the knee in running". Journal of Biomechanics, 35(11), pp. 1459–1474.

[47] B. Colobert, A. Cretual, P. Allard and P. Delamarche, 2006. "Force-plate based computation of ankle and hip strategies from double-inverted pendulum model". *Clinical Biomechanics*, 21(4), pp. 427–434.

[48] S. Sasimontonkul, B.K. Bay M.J. and Pavol, 2007. "Bone contact forces on the distal tibia during the stance phase of running". *Journal of Biomechanics*, 40(15), pp. 3503–3509.

[49] W. Blajer, K. Dziewiecki and Z. Mazur, 2007. "Multibody modeling of human body for the inverse dynamics analysis of sagittal plane movements". *Multibody System Dynamics*, 18(2), pp. 217–232.

[50] A.R. Meyer, M. Wang, P.A. Smith and G.F. Harris, 2007. "Modeling initial contact dynamics during ambulation with dynamic simulation". *Medical and Biological Engineering and Computing*, 45(4), pp. 387–394.

[51] F. Iida, J. Rummel and A. Seyfarth, 2008. "Bipedal walking and running with spring-like biarticular muscles". *Journal of Biomechanics*, 41(3), pp. 656–667.

[52] K. Kutzbach, 1929. "Mechanische leitungsverzweigung; ihre gesetze und anwendungen". *Maschinbau der Betrieb*, 8(21), pp. 710–716.

[53] G. Wu, S. Siegler, P. Allard, C. Kirtley, A. Leardini, D. Rosenbaum, M. Whittle, D.D. D'Lima, L. Cristofolini, H. Witte, O. Schmid and I. Stokes, 2002. "ISB recommendation on definitions of joint coordinate system of various joints for the reporting of human joint motion—Part I: ankle, hip, and spine international society of biomechanics". *Journal of Biomechanics*, 35, pp. 543–548.